Correlation of Damage Rating Index in Concrete Pavements

by

Ali Qutail

Submitted in Partial Fulfillment of the Requirements

For the Degree of

Master of Science in Engineering

In the

Civil and Environmental Engineering Program

YOUNGSTOWN STATE UNIVERSITY

May 2021

Correlation of Damage Rate Index in Concrete Pavements

Ali Qutail

I hereby release this thesis to the public. I understand that this thesis will be made available from the OhioLINK ETD Center and the Maag Library Circulation Desk for Public access. I also authorize the university or other individuals to make copies of this thesis as needed for scholarly research.
Signature:

_____

Ali Qutail, Student Date

Approvals

_____

Dr. Richard A. Deschenes, Thesis Advisor Date

_____

Dr. AKM. Anwarul Islam P. E., Committee member Date

_____

Dr. Suresh Sharma, Committee Member Date

_____

Dr. Salvatore A. Sanders, Dean of Graduate Studies Date

ABSTRACT

Alkali-silica reaction (ASR) is a considerable durability issue in concrete. Concrete may expand and crack due to ASR, which affects the mechanical properties and permeability of the concrete. The aim of this project was to study the effect of three compressive stress states on the development and distribution of expansion and deterioration in externally restrained concrete pavements. Nine concrete cubes (10 inches [254 mm]) were cast in the Concrete Materials Lab at Youngstown State University. A mixture design typically of concrete pavements was used to simulate the characteristics of highway pavements. Subsets of three cubes each were cast to evaluate three different confinement states: (1) no confining stresses (unrestrained), (2) uniaxial confining stresses (uniaxial restraint), and (3) biaxial confining stresses (biaxial restraint). All nine cubes were stored in an environmental chamber with a relative humidity of 95-100% and temperature of 38º C (100 º F). The uniaxially restrained cubes were confined by a 5 MPa (725 psi) stress along one axis. The biaxially restrained cubes were also confined by a 5 MPa (725 psi) stress along one axis and 4 MPa (580 psi) stress along the perpendicular axis. The strain of each cube was measured bi-weekly over a period of 416 days (Expansion Test). One cube from each subset (stress state), was removed from the rotation when specific strain values were reached: 0.15%, 0.25% and 0.35%. These samples from each stress state were cut and prepared for damage rating index (DRI) measurements. The expansion test results indicate less volumetric strain in the restrained cubes. DRI test results indicate that confining stress reduced deterioration in the planes perpendicular to the confined axes. Overall, the results indicate that expansion is not transmitted to the unrestrained axes, while cracking perpendicular to the restraint is inhibited.

Acknowledgement

First, I must thank my parents Mohammad and Fatima Qutail for supporting me since I was born until now. I also thank my uncle Adnan Qutail for sponsoring and supporting me. He always motivated me to improve my education and gain a master's degree in civil engineering. My wife Nicole deserves a lot of love, appreciation, and thanks for helping me to be able to finish writing this thesis.

I would like to thank my thesis advisor Dr. Richard Deschenes for everything he has done for me and all other students. He was always very helpful and so generous in explaining and discussing all situations and problems I have countered. His office door was always open for all students from all engineering departments. In addition to that, he is well educated not only in civil engineering but also in many related disciplines.

I would like to thank Dr. AKM Anwarul Islam, Dr Suresh Sharma for being committee members for this thesis. Also, I want to thank all faculty members that provided me any kind of help or support.

Finally, I want to thank the college of graduate studies for giving me a scholarship. I also thank the department of civil and environmental engineering for hiring me as a teacher assistant for two years, which gave me a lot of experience.

Table of Content

List of Tables

List of Figures

1 Introduction

1.1 Background

Alkali Silica Reaction (ASR) is a concerning source of concrete durability and serviceability problems (FHWA, 2010). It is a deleterious reaction between the alkaline pore solution of concrete and certain silicious phases in aggregates (Hobbs, 1988; Poole, 1992; Thapa, 2018). The reaction produces swelling gels that absorb moisture and swell, which may result in tensile cracking in concrete structures. ASR has been studied for more than nine decades. Many researchers have studied the reaction mechanisms and the factors that affect its rate, which are summarized herein (Stanton, 1940; Fournier, 2000). The occurrence of ASR requires the availability of reactive silica (SiO_2), alkalis (Sodium (Na), Potassium (K)), and moisture (H_2O) (Rajabipour et al., 2015; Thapa, 2018). The rate of ASR depends primarily on exposure conditions (relative humidity and temperature), aggregate properties, pore solution composition, and stress states (Allford, 2016; Gautam, 2017; Giaccio, 2018).

When ASR occurs in concrete pavements, the confining stresses due to external and internal restraint may induce a redistribution of expansion (strain) and deterioration. Therefore, studying the progression of ASR in concrete with uniaxial and biaxial restraint is important to further understand ASR deterioration in concrete pavements. Allford (2016) and Gautam (2017) investigated the effect of various degrees of external restraint on the progression of ASR deterioration in concrete. The present study considers external restraints analogous to those found in concrete pavements, with the goal of further understanding the distribution of strains and deterioration in pavements. To quantify the degree of deterioration occurring in concrete along the restrained and unrestrained

dimensions, expansion (strain) and the damage rating index (DRI) were used. The DRI method was developed to quantify the internal deterioration due to ASR. It can be applied to laboratory specimens (cylinders or cubes) or on cores taken from existing structures (Dunbar and Grattan-Bellew, 1995; Grattan-Bellew and Mitchel, 2006).

1.2 Scope

The goal of this research is to understand the effects of three different stress states on concrete pavements undergoing alkali-silica reaction (ASR). First, the mechanical properties (strength and 7modulus of elasticity) of cylindrical specimens were tested. The accelerated mortar bar test (AMBT) was used to test the reactivity of the aggregates used in this research. Next, nine cubes (10 in [254mm]) were constructed from concrete with characteristics comparable to mixtures used in concrete pavements. Three cubes were constructed with no restraint, three cubes were constructed with a restraint of 5 MPa (725 psi) along the one axis, and three cubes with two different restrains of 5 MPa (725 psi) and 4MPa (580 psi) along perpendicular axes. The strain along all three perpendicular axes of each cube was measured bi-weekly to quantify the differences in expansion between the three stress states and in each direction. When the average strain in the unrestrained cubes reached 0.15%, three of the nine cubes (one from each stress state) were cut and polished for DRI testing. When the average unrestrained cubes reached 0.25%, an additional three cubes were removed for the DRI test. The DRI of the last three cubes was measured when the average strain in the unrestrained cube reached 0.35%

1.3 Research Organization

This thesis is organized as follows: First, Chapter 2 is an extensive literature review and includes the definition and requirements for alkali-silica reaction (ASR). Also, the

discussion includes the chemical, environmental, and physical factors that affect the rate and severity of the ASR. Several methods for preventing and controlling ASR, used and tested by other researchers to control or prevent ASR, are discussed as well. Finally, some of the key research from the last two decades is discussed and summarized in the final portion of the literature review. Chapter 3 is a summary of the experimental methods for the laboratory testing, expansion measurements, and DRI testing. Mechanical testing included the modulus of elasticity and strength of cylindrical specimens. The ASR tests included the accelerated mortar bar test (AMBT), the concrete prism test (CPT), expansion measurements and the Damage Rate Index (DRI). A detailed test procedure for all test methodologies is provided including the mix design, materials, apparatus, and measurements. Chapter 4 summarizes the results and the data analyses of all testing performed herein and a discussion on the outcomes. Chapter 5 summarizes the key outcomes and findings of the research. Finally, the raw collected data and results were tabulated and organized in the appendix.

2 Literature Review

2.1 Alkali-Silica Reaction (ASR)

ASR is one of the two alkali-aggregate reactions (AAR) that is a main cause of concrete durability and serviceability problems (FHWA, 2010). AAR is a deleterious reaction between the alkaline pore solution of concrete and silicious phases in aggregates (Hobbs, 1988; Poole, 1992; Thapa, 2018). The reaction produces swelling gels that absorb moisture, swell, which may result in tensile cracking in concrete structures. ASR has been studied for more than nine decades and has been recorded in more than 50 countries worldwide (Stanton, 1940; Fournier, 2000).

2.2 ASR Requirements

The chemical and physical reaction mechanisms at the molecular to micro-scale are not well understood, resulting in the inability to assess the risks and predict the service life of structures undergoing ASR (Rajabipour et al., 2015). According to most ASR studies in the past, the occurrence of ASR requires the availability of reactive silica (SiO_2), alkalis (Sodium (Na), Potassium (K)), and moisture (H_2O) (Rajabipour et al., 2015; Thapa, 2018).

2.3 Factors

ASR is affected by several factors that may change the rate and the magnitude of the gel formation and expansion mechanisms (Molchanov, 1957; Walther, 1977; Fournier, 2010; Giaccio, 2018). Those factors can be categorized as aggregate properties, pore solution chemical composition, and exposure conditions (Rajabipour et al., 2015; Allford, 2018).

2.3.1 Aggregate Properties

Aggregate, as the principle reactive phase in ASR, necessitate understanding its interaction in concrete to improve our understanding of the ASR reaction and how it is mitigated (Rajabipour et al., 2015). Some standardized tests, such as the accelerated mortar bar test (AMBT) and concrete prism test (CPT) are currently used to classify aggregates (or concrete mixtures) into four different reactivity levels: non-reactive, moderately reactive, high reactive, or highly reactive aggregates (Shehata, 2000; Thapa, 2018).

2.3.1.1 Aggregate Composition and Mineralogy

Aggregates are composed of multiple minerals and phases that may influence the rate and magnitude of ASR. Various minerals are known for their potential reactivity. Amorphous silica (opal), chert, flint, shale, rhyolite, and marl are examples of reactive minerals. Meta-stable and microcrystalline silica phases are less reactive than amorphous silica (Diamond, 1976; Poole, 1992, Mehta, 2002; Giaccio et al., 2008). All the above minerals are examples of reactive minerals that may lead to a moderate to severe ASR related deterioration in concrete. Results of the ASR reaction can be visible in less than a year in certain aggressive environmental conditions (e.g., warm, humid conditions). On the other hand, some less-reactive minerals, e.g., polycrystalline and strained quartz, may need decades to induce the reaction (McConnell, 1947; Bellew, 1989; Batic, 2002; Giaccio et al., 2008). Researcher indicates that the amount of reactive silica necessary to trigger the expansion is at least 5kg/m^3 (Diamond, 1983; Rivard et al., 2007, Multon et al.,2009).

2.3.1.2 Aggregate Size

ASR gel formation and expansion rates are not typically considered a function of particle size. It is to be expected that a smaller particle size would contribute to a faster

ASR rate as it increases the reaction surface area (Stanton, 1940; Vivian, 1951; Rajabipour et al., 2015). Contrarily, most experiments and reported observations indicate that deleterious reactions occur when using particle sizes ranging from 0.18 mm to 10 mm (Stanton, 1940; Jin et al., 2000; Multon et al., 2008). Many hypotheses have been set forth to explain the phenomena of the intermediate/pessimum aggregate size effect. The proposed explanation for this pessimum particle size is the availability of certain mineral phases which result in a pozzolanic reaction, that would otherwise be unavailable for reaction in larger particles. This explanation fails to justify the observations found with larger particles (Diamond, 1974; Shao et al., 2000).

2.3.1.3 Reactive Aggregate Content and Intraparticle Reaction

ASR expansion typically increases proportionally with reactive aggregates until the maximum (pessimum) content is reached. However, the expansion decreases with higher reactive aggregate content. It is suggested by multiple researchers that the maximum content is achieved when the ratio of reactive silica to alkalis is around 6 (Hobbs, 1979; Glasser, 1981; Moundoungou, 2014). At higher ratios, the higher rate of silica dissolution results in less expansion.

The accessibility of the alkaline pore solution to the reactive silica also plays a role in ASR rate and magnitude. Therefore, the rate of ASR increases proportionally with interior micro-cracks in aggregates. Also, the reactive minerals availability on the surface of aggregate may influence the rate of expansion because ASR gels forms more readily on the surface. On the other hand, when reactive silicas are absent on the surface, the ASR process is much slower and may require many years to develop (Lane, 1994; Hou et al., 2004; Maragechi et al. 2012).

2.3.2 Pore Solution Chemical Composition

Alkalis (K, Na), calcium, lithium, aluminum (and other constituents) are available in typical concrete pore solutions and originate from different sources (cement, fine and coarse aggregate, and admixtures). Cement is the primary source of alkalis in concrete mixtures, followed by aggregate, and possibly supplementary cementitious materials (SCMs) that may also contribute to other deleterious reactions (Rajabipor et al., 2015). Effective alkalis within the pore solution are required to maintain the hydroxyl ion concentration, which is necessary to maintain the dissolution of silica and formation of gel (Diamond, 1983; Kollek, 1986). The primary types of alkali cations necessary in pore solution (i.e., Na, K, Ca, and Li) have different effects on the mechanism of ASR. While Na, K, and Ca are necessary for swelling gels to occur, excess of Ca and Li can result in non-swelling gels (Rajabipor et al., 2015).

2.3.3 Exposure Conditions

Relative humidity (RH) is the most fundamental exposure condition that is required for ASR expansion to occur, as the expansion process requires a replenishing source of water. Temperature and other exposure conditions effect the rate of the reaction. Some ASR reactions need decades to show visible symptoms (e.g., cracking and gel exudation), but by controlling humidity and temperature, the time required for visible distress may be reduced to a few years or months (Helmuth, 1970; Hansen, 1987; Multon, 2009). RH greater than 80% is typically ideal to facilitate ASR expansion. When the RH is sustained at values less than 80%, ASR gel formation may occur, but swelling will be slowed (or stopped) until RH returns to around 80-85%. Some authors suggested that the peak expansion requires an RH of at 95% (Allford, 2016). Higher ambient temperature typically

increases the rate of ASR gel formation since the solubility of SiO_2 also increases with temperature. As an example, the solubility of α-quartz at a temperature of 75°C is roughly five times the solubility at 25°C (Walther, 1977; Poole, 1992; Hobbs, 2009).

2.4 ASR Mechanism

Since the discovery of ASR in the 1940's, explaining the mechanism of ASR has been of great interest for many researchers and institutes worldwide. As a result, the industry has come to understand the ASR mechanism and reaction environment well enough to develop mitigation and prevention methods (Wang, 1991). A multitude of articles have been published regarding the silica dissolution process, which has led to a clearer understanding of the ASR mechanism (Rajabipour, 2015). In summary, the reaction mechanism originates with the dissolution of unstable silica (under the action of alkaline pore solution), followed by the formation of silica solution and then silica gels. After this (and when the alkali concentration is sufficient), swelling gels absorb moisture resulting in swelling of the gel product and then generating tensile stresses that may result in microcracking of the concrete (Brantly, 2008).

Due to the instability of silica in aggregates, silicas may dissolve in the pore solution. Typically, a pH around 9 or 10 will result in a relatively constant silica solubility, while the pH of concrete pore solution is typically closer to 12-13. The solubility of silica rapidly increases nonlinearly as the pore solution pH increases (Urhan, 1987; ISE, 1992; Multon et al., 2009; Allford, 2016). At higher pH, dissolved silica will react with alkali ions (k^+ and Na^+), forming ASR gels. Resulting gels will absorb moisture due to the osmotic pressure gradient between ASR gels and the pore solution. When moisture is absorbed from the pore solution by silica gels, the volume increases, and gels generate

pressure on unrestrained axis resulting in concrete micro-cracks (Swamy, 2002; Gautam, 2016; Thapa, 2018).

2.5 ASR Prevention

Rajabipour et al. (2015) provided a very insightful summary of the current understanding of ASR and the knowledge gaps. He explained the many factors that are known to affect the reaction and detailed the chemical equations of the reaction and its environment. Multiple methodologies were suggested to control or prevent the reaction. Rajabipour et al. (2015) recommended that researchers focus on quantifying the thermodynamics and kinetics data to determine the aggregate composition and heterogeneity. They also concluded that aggregate reactivity is affected by the size and distribution of the minerals within its structure. The lithium compound, $LiNO_3$, was considered as an ASR controller, but they recommended more research to figure out the mechanism of why Li controls the ASR. The following information is a summary of the methods for preventing and controlling ASR.

ASR often requires more than ten years to show visible distress in concrete structures. It starts with silica dissolution, which takes multiple years and appears when silica gels swell and generate sufficient pressures that micro-cracks the concrete components. ASR may occur more rapidly some severe exposure conditions. It is sometimes necessary to prevent ASR occurrence or at least minimize its severity. In some countries, there is a limit of the alkalis content in the concrete mix. It has been recommended that an alkali content of 2.0-4.00 kg/m^3 will be safe to prevent ASR with most reactive aggregates. The reaction may still occur, but it will likely not be destructive reaction (Nixon, 1992; Thomas, 1996; Berra et al., 1999). When CaO is absent, reactive

silica dissolves without any destructive damage since it is necessary to have calcium-rich gels to cause damages (Diamond et al., 1989, Thomas, 1998). Therefore, limiting the availability of calcium in pore solution, by binding calcium within secondary hydration products, may reduce the severity of ASR. Therefore, admixtures which produce secondary hydration products (e.g., fly ash or slag cement) are often employed to prevent ASR.

Field experience and laboratory tests have shown that using sufficient quantities of fly ashes can minimize ASR expansions in concrete (Thomas, 1996; Shehata, 2000). AMBT and CPT testing has been used to study and evaluate the efficacy of specific fly ashes in mitigating and preventing ASR in concrete. Certain types of fly ashes, specifically low calcium fly ashes, were found to be effective in reducing ASR expansions as they potentially reduce the alkalinity of the pore solution, refine the pore structure, and bind alkalis and calcium within secondary hydration products (Shehata, 2000).

Some lithium compounds (e.g., LiOH, $LiCO_3$, and $LiNO_3$) are used to control ASR expansions. Further studies are needed to understand the mechanism of how such compounds regulate ASR expansion. Lithium tends to reduce the solubility of reactive silica and the formation of silica gels. Thereby reducing swelling of silica gels and consequently ASR expansion (Sakaguchi et al., 1989; Stark, 1992; Collins et al., 2004; Feng et al., 2010).

2.6 The Effect of External Restrain on ASR Expansion

The aim of the present study is to better understand the effects of external restraint on the distribution of expansion and deterioration in concrete. Uniaxial and biaxial restraint have been shown by Multon et al., (2005), Allford, (2016), and Gautam, (2017) to potentially result in strain redistribution into the unrestrained direction. These past research

efforts are summarized below to inform the present study and to identify knowledge gaps relevant to the present research.

2.6.1 Multon, 2005

Multon (2005) studied and discussed the effect of various stress states on ASR expansion. He used a standard concrete mix design with a water to cement ratio of 0.5 in two mixtures. One of those mixtures contained reactive silicas, while the other did not contain any reactive phases. The axial and radial strains were measured at different confining stress states of 0, 10, and 20 MPa (0, 1450, 2901 psi) for both mixtures. Multon (2005) observed that ASR volumetric strain is constant under the studied stress states. In addition, he demonstrated that expansions were transferred to the unloaded direction (stress-free directions).

2.6.2 Allford, 2016

Allford (2016) concentrated his research on ASR in reinforced concrete specimens. Thirty-nine concrete cubes were built in the lab with either no reinforcement, uniaxially reinforcement, biaxially reinforcement, and triaxially reinforcement. The steel ratio varied from 0.49% to %1.50% to find a relationship between axial expansions and steel ratio. Concrete cylinders and prisms were made using the same mixtures used in the cubes for comparison purposes and strength tests. Axial expansion data were collected over time and showed that the steel ratio does not influence expansions. Cubic specimens had higher expansion rates affected by different lab exposure conditions where those tests were conducted. Allford (2016) reported that larger cracks appeared in the unreinforced face, which were parallel to the reinforcement. This is caused by the relatively lesser restraint perpendicular to the reinforcement, allowing the concrete to expand and cracks to open

parallel to the reinforcement direction. One of the most important findings was that expansions in the unreinforced direction were always more than expansions in other directions. In addition to that, expansions in the unreinforced direction were half of the total volumetric expansions. The explanation for this observation, was the redistribution of expansion into the unrestrained direction.

2.6.3 Gautam et al., 2017

Gautam and his colleagues published two papers in 2017 concerning expansion in externally restrained concrete. They studied ASR in multiaxially restrained concrete specimens, with external post-tensioning. Unlike Multon (2016), the steel restraint was external post-tensioning intended to simulate conditions found in nuclear power plants. Gautam et al. (2017a) discussed the relationships between stress states and expansions. Gautam et al. (2017b) provided details about the Damage Rating Index (DRI) test conducted on the samples. The findings were as follows:

(i) Stresses reduce the expansions and expansions are transferred to the unstressed directions.

(ii) Triaxial stresses slightly reduced the volumetric expansions, but they do not totally eliminate the expansion.

(iii) In the cases where one or more directions are unrestrained, stress is not sufficient to reduce the volumetric expansions since expansion continues to occur in the free (unrestrained) directions.

(iv) Cubes that were not restrained in any direction showed less compressive strength due to greater cracks caused by ASR.

2.7 ASR Outcomes

ASR is a destructive reaction that threatens concrete structures throughout the world (Gautam et al., 2017). The reaction outcomes are complicated by various interacting factors, and yet to be fully understood (Thapa, 2018). The factors can be broadly categorized as (1) gel expansions, (2) aggregate and cement paste cracking, and (3) mechanical properties degradation (Multon, 2006; Gautam et al., 2017).

Expansion starts in concrete components undergoing ASR once the silica gels are produced. Those gels begin to imbibe moisture from the pore solution due to the difference in osmotic pressures between gels and the pore solution (Swamy, 2002; Thapa, 2018). Multiple researchers have concentrated on expansions in ASR-affected structures, trying to better understand the mechanism and factors that might affect the magnitude and rate of the expansion (Shehata, 2000; Multon, 2006). Some researchers considered that restraint may be effective in reducing ASR expansions. They have since published a variety of results based on expansion and DRI testing to assess expansions in the restrained and unrestrained directions (Kawamura, 2004; Multon, 2006; Dunant, 2010; Kagimoto et al., 2014; Gautam et al., 2017; Thapa, 2018).

ASR gels have been demonstrated to expand, generating tensile stresses with a range laying between 2.75 MPa (400 psi) to 10MPa (1450 psi), exceeding the tensile strength of the concrete and potentially external or internal restraint. Microcracks start within aggregates and proceed in the cement paste before they appear on the surface producing cracking maps (Wang, 1991; Rajabipour et al., 2015; Thapa, 2018). The DRI has been considered as the most promising quantitative methodology to quantify ASR

deterioration within concrete, and the distribution of cracking in different restrained and unrestrained directions. (Rivard et al., 2009; Sanchez et al., 2015).

Expansions, microcracks, and macrocracks due to ASR can affect the mechanical properties of concrete (Allford, 2016). Studying the degradation of the concrete mechanical properties is essential to evaluate the safety and serviceability of ASR-affected structures (Gautam et al., 2017). Many researchers have investigated the effect of ASR on concrete mechanical properties. Most of them concluded that ASR reduced the tensile strength and the modulus of elasticity of the tested specimens. However, deleterious expansion did not change the compressive strength until larger expansions had occurred. (Swamy, 1988; Marzouk, 2003; Giaccio et al., 2008; Allford, 2016).

2.8 Test Methods

A variety of expansion test methods have been developed to assess the potential reactivity of aggregates and concrete mixtures. These tests are primarily used to assess the potential for deleterious expansion for an aggregate or concrete mixture. However, these methods are typically limited to predicting the performance of an aggregate or concrete mixture, but not the mechanical deterioration, rate of expansion, or long-term performance of concrete. Some of the relevant test methods are summarized below.

2.8.1 Accelerated Mortar Bar Test (AMBT)

The AMBT is a methodology specified in ASTM C1260 Standard Test Method for Potential Alkali Reactivity of Aggregates (Mortar-Bar Method), which has been developed to classify aggregates as: non-reactive, moderately reactive, highly reactive, or very highly reactive (CAN/CSA-A23.2-27A-09, 2009; AASHTO PP 65-11, 2013; Rajabipour et al., 2015). The AMBT test method is widely used because results can be obtained within 16-

30 days (Shon et al., 2002). Standardized aggregate graduation and mixture design requirements are specified within ASTM C1260, and used to prepare and cast the mortar bars. The standardized mixture design includes a w/c of 0.47 with 440 g of water and 990 g of fine aggregates. Standard molds are used to produce mortar bars of 25x25x285mm dimensions, with embedded metal studs on each end to facilitate measuring length change. Mortar bars are cast and moist cured for 24±2 hours at 23±2 ºC. The bars are then stored in water at 80±2 ºC for 24±2 hours, to accelerate curing. At this point, the initial length readings of all bars are recorded using a length-change apparatus, with a precision of ±0.002 mm before they are moved into a 1 N NaOH solution. The length-change is periodically recorded over 14 days, while ensuring the temperature remains at 80±2 ºC. Based on the final expansion, specimens are classified as shown in **Table 2-1**.

Table 2-1, Aggregate Classification Using the AMBT (ASTM C1260)

Expansion at 14 days	**Classification**	**Notes**
Less than 0.10%	Non-reactive to reactive	Innocuous reactivity
0.10% - 0.20%	Moderately reactive	Potentially deleterious reactivity
More than 0.20%	Highly to very highly reactive	Deleterious reactivity

2.8.2 Concrete Prism Test (CPT)

The CPT (in accordance with ASTM C1293 Standard Test Method for Determination of Length Change of Concrete Due to Alkali–Silica Reaction) differs from the AMBT, in that concrete mixtures containing coarse aggregates can be tested as compared to representative mortars. The CPT is the primary and preferred test method used to understand the behavior of concrete containing reactive aggregate and mitigation measures (Rajabipour et al., 2015). **Table 2-2** below is a summary of the required mix design provided in ASTM C1293. It is also required to maintain the water to cement ratio

of 0.42 to 0.45 (ASTM C1293). The coarse aggregate fraction was determined from 0.7±0.02 of the dry rodded unit volume of the aggregate to be used, which was graded following the requirements in **Table 2-2**.

Table 2-2, Mix Design for CPT (ASTM C1293)

Material	Cement	Coarse aggregate	Fine Aggregate	w/c
Weight (kg/m^3)	420±10	0.33 - 4.75-9.5 0.33 - 9.5-12.5 0.33 - 12.5-19.0 mm	Determined by Absolute Volume	0.45

Three 75x75x285mm concrete prism specimens were cast and then stored for 24±10 hours before being unmolded. The storage environment is maintained at a temperature of 38±2ºC and a RH of 100±5%. Prisms should be kept in sealed plastic containers over time. Containers are moved to an area of 21 ºC temperature for at least 12 hours (but not more than 20 hours) before length-change readings are taken. Readings are taken immediately after unmolding, and then at 7, 28, 56 days, 3, 6, 9, 12, 24 months.

2.8.3 Compressive Strength and Modulus of Elasticity

The compression and modulus of elasticity tests are a good indicator of the mechanical properties of concrete specimens. It is required that the compressive strength (ASTM C39 Standard Test Method for Compressive Strength of Cylindrical Concrete Specimens) be carried out first since its outputs are needed to conduct the modulus of elasticity test (ASTM C469 Standard Test Method for Static Modulus of Elasticity and Poisson's Ratio of Concrete in Compression). A standard rated axial compressive load is applied on cylinders until failure is reached. The maximum compressive load is then divided by the cross-sectional area of a specimen to determine the cylindrical concrete specimen compressive strength (ASTM C39). After that, the standard modulus of elasticity test is conducted at least twice on every sample up to 40% of the compressive strength

recorded in the compressive strength test. The testing machine should be capable of maintaining a continuous loading pattern with a rate laying between 0.24±0.05 MPa/sec (35±7 psi/sec) in hydraulically operated machines. The modulus of elasticity is recoded to the nearest 50,000 psi (ASTM C469).

2.8.4 Damage Rating Index Test (DRI Test)

DRI was proposed in the 1990s as a semi-quantitative petrographic method to assess the internal damages in concrete (Dunbar and Grattan-Bellew, 1995; Grattan-Bellew and Mitchel, 2006). It has been used to quantitatively assess damages due to alkali-aggregate reactions (AAR) e.g., alkali-silica reaction (ASR), delayed ettringite formation (DEF) and freeze-thaw (FT) cycles (Bérubé et al., 2012; Sanchez et al., 2020). The DRI method can be used to assess internal damages in lab-made samples or cores taken from existing structures (Rivard and Ballivy, 2005).

The test procedure involves first cutting samples from the specimen, then polishing the surface using a hand-polisher. A grid of 1 cm^2 squares is drawn on the concrete surface. Then, A 15-16x magnification stereomicroscope is used to analyze each 1 cm^2 cell on the concrete surface. The primary ASR deterioration features present on at least 200 cm^2 of the surface are counted to quantify the internal deterioration. Each ASR deterioration feature is multiplied by a weighing factor. The final DRI is the summation of all features normalized to a 100 cm^2 surface area. The commonly agreed upon weighing factors from the literature are summarized in **Table 2-3** (Villeneuve et al., 2012; Sanchez et al., 2020).

Table 2-3, ASR Features and Weighing Factors for DRI Test

ASR petrographic features	Weighing factor
Closed cracks in coarse aggregate particles (CCA)	0.25
Open cracks in coarse aggregate particles (OCA)	2.00
Open cracks in coarse aggregate particles with gels (OCAG)	
Disaggregated aggregate particles (DAP)	
Cracks in cement pate (CCP)	3.00
Cracks in cement paste with gels (CCPG)	
Debonded coarse aggregate (CAP)	

3 Experimental Methods

To further understand the effect of external restraint on ASR in concrete pavements, a regimen of six test methods were used to understand the mechanical performance, rate and potential for expansion, and distribution of deterioration in the concrete. The mechanical properties of the concrete tested included the strength and modulus of elasticity of cylindrical specimens. The accelerated mortar bar test (AMBT) and the concrete (CPT) were carried out to catalog the reactivity of the reactive Jobe-Newman sand used herein. Finally, the expansion and deterioration of concrete with three different stress states were evaluated using strain measurements and the damage rate index (DRI).

3.1 AMBT (ASTM C1260)

The accelerated mortar bar test (AMBT) is carried out to classify aggregates according to their reactivity using standard mortar bars. It is a rapid method that provides results in a period of 16-30 days only (ASTM C1260). The Jobe-Newman sand (from El Paso, TX) was evaluated following the AMBT method. A non-reactive sand from Youngstown Ohio was also tested. These two aggregates were blended in the concrete mixtures used herein to produce an expansive concrete mixture, with a lesser rate of expansion. The alkali content in cement does not affect AMBT results, which are only an index of potential for expansion since the mortar bars are immersed in the NaOH solution. ASTM C1260 requires fine aggregates grading, as shown in **Table 3-1**.

Table 3-1, Grading requirements for AMBT (ASTM C1260)

Sieve Size (mm)		
Passing	**Retained on**	**Mass, %**
4.75	2.36	10
2.36	1.18	25
1.18	0.60	25
0.60	0.30	25
0.30	0.15	15

The temperature of the molding room should be maintained between 20 °C and 27.5 °C (Mixing water temperature and surrounding moist temperature should be 23 ± 1.7 °C). The concrete was cured in the molds for 24 hours and then the mortar bars were stored in containers and totally immersed in water for 24 hours and then 1N NaOH solution for the remining 28 days. The specimen containers should be durable under the 1N NaOH solution and 80 ± 2 °C conditions, as shown in **Figure 3-1**. Finally, the storage temperature of the mortar bars should be maintained between 78 °C and 82 °C.

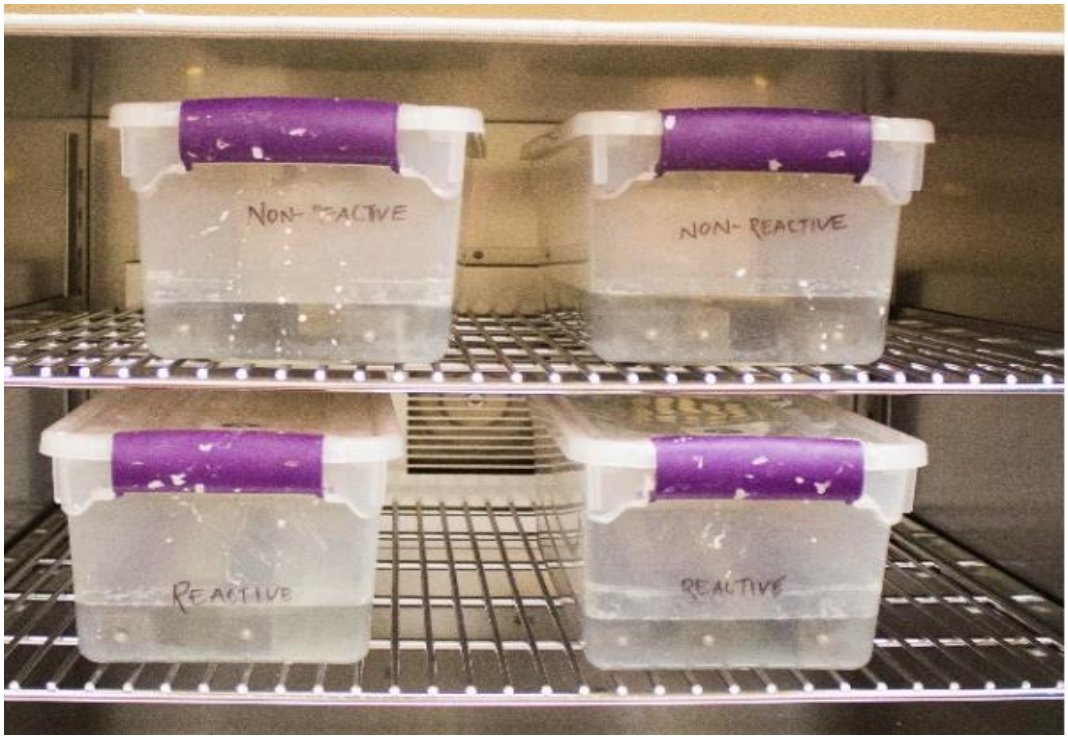

Figure 3-1, Storing AMBT specimens in 1N NaOH resistant containers (picture by Romit Thapa)

For each aggregate tested, six specimens were cast, as shown in **Figure 3-2.** After curing, at least three axial expansion readings are required over a 14-day period. It is preferred to record expansions at the same time each day. In this experiment, expansion values are taken for the Jobe-Newman sand and non-reactive (Youngstown) sand to compare the expansion results over a 14-day (or 28-day) period. The mix design, as summarized in **Table 2-1**, was used to batch and cast six mortar bars for each aggregate.

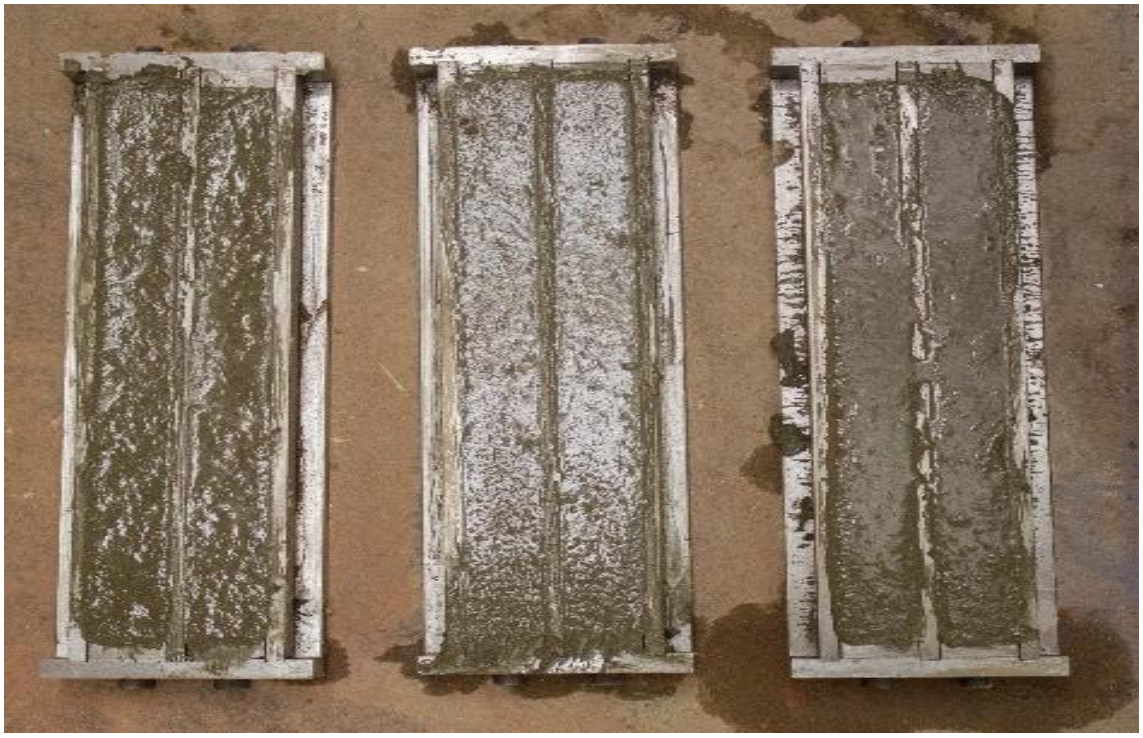

Figure 3-2, AMBT in-mold specimens (picture by Romit Thapa)

3.2 CPT (ASTM C1293)

The Concrete Prism Test (CPT) is followed to determine the tendency of an aggregate and concrete mixture to cause expansive ASR. Type I Portland cement (meeting ASTM C150) should be used in all mixtures. Per ASTM C1293, the cement alkali content should be between 0.80% and 1.00%. The concrete mixture alkali content should be further

boosted to 1.25% NaOH equivalents. NaOH pellets are added to the mixing water to achieve the required mixture alkali content. The mix design used was previously provided in **Table 2-2**. The grading requirements specified in ASTM C1293 were followed. A mixture containing a blend of Jobe-Newman and Youngstown sands (40/60 percent by weight) was cast to produce six concrete prisms. After curing, length change measurements were taken following the procedure summarized previously in **Chapter 2.8.2**. **Figure 3-3** below shows the containers used to store the prisms and the micrometer used to measure the length changes.

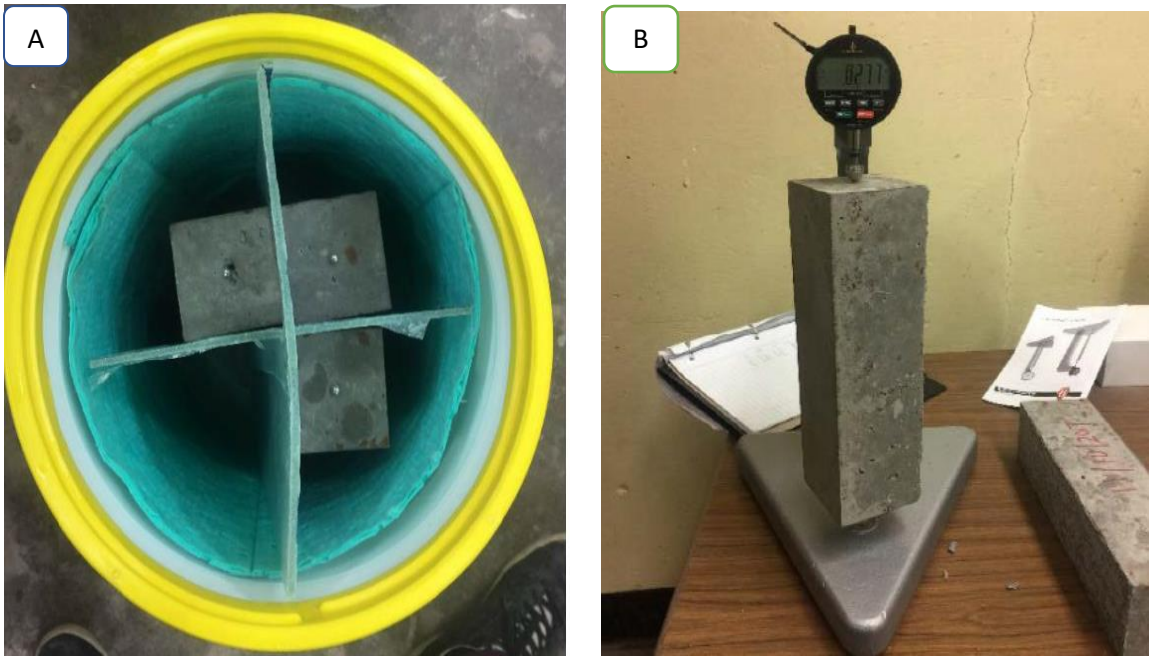

Figure 3-3, Concrete Prism Test (CPT) (a) Storing concrete prisms in plastic containers. (b) A prism length change measurement using a micrometer. (pictures by Romit Thapa).

3.3 Compressive Strength and Modulus of Elasticity of Cylindrical Specimens

The compressive test (ASTM C39) and the modulus of elasticity (ASTM C469) results were used to determine the mechanical properties of concrete specimens, prior to deterioration. The average compressive strength of six different specimens were used to determine the compressive strength of the concrete, which was necessary before testing the

modulus elasticity. The modulus of elasticity of the remaining specimens were tested up to 40% of the average compressive strength. **Figure 3-4** shows a cylinder that was tested until failure to calculate the compressive strength. Then another cylindrical specimen was tested up to 40% of the compressive strength, as shown in **Figure 3-5**.

ASTM C39 and ASTM C469 require a testing machine capable of providing a specified loading rate (ASTM C39 and ASTM C469). The loading should be continuous without shock. The loading rate is 0.05 in/min, which is equivalent to 0.24±0.05 MPa/sec (35±7 psi/sec) in hydraulically operated machines.

Figure 3-4, A cylindrical specimen failed under a compressive load. (picture by Romit Thapa)

Figure 3-5, A cylindrical specimen is undergoing the modules of elasticity test. (picture by Romit Thapa)

3.4 Expansion Test

A pavement mix design was used to cast three sets of 10-in cubes. The expansion along each axis of the nine cubes were measured periodically over 416 days. Then the DRI test, a semi-quantitative petrographic method, was performed to assess the internal deterioration in concrete due to ASR. The nine cubes were divided to three subsets, with different stress states (three cubes in each set). The DRI test was performed on one cube of each set once the average strain reached 0.15, 0.25 and 0.35 percent.

3.4.1 Mix Design

A blend of Jobe-Newman and Youngstown sands (40/60 percent by weight) and non-reactive coarse aggregate were used in the expansion and the DRI tests. Jobe-Newman is highly reactive sand from El Paso, Texas (ASTM C1778). The non-reactive coarse

aggregate was a ¾-in. (nominal maximum size) crushed limestone from Youngstown, Ohio. The Jobe-Newton sand is primarily composed of quartz, feldspars, chert, and other siliceous volcanic phases. A high-alkali cement (ASTM C150 and AASHTO M85) was used in all experiments. The cement was supplied by Lehigh Heidelberg Cement Group with a chemical composition shown in **Table 3-2**. The Na_2O_{eq} of this cement was 0.84%, which was boosted to 1.25% in the final mixture.

Table 3-2, Cement Composition

CaO	SiO_2	Al_2O_3	Fe_2O_3	SO_3	MgO	C_3S	C_3A	Na_2O_{eq}
62.38%	20.06%	5.21%	3.01%	3.43%	2.21%	52.42%	8.70%	0.84%

The concrete mixture design was based on a typical pavement mixture design and was used for all cube specimens herein. The cement content was 564 lb/yd^3 with a water to cement ratio of 0.47. The natural gradation of the coarse and fine aggregate was used. **Table 3-3** below summarizes the pavement mix design used for the expansion and the DRI tests.

Table 3-3, Mix Design Used in Expansion Test and DRI Test

Material	Cement	Coarse Agg.	Fine Agg.	Water
Content (lb/yd^3)	564	1850	1318	265

3.4.2 Materials and Cubes Preparation

A ¾-in. thick plywood was used to make detachable formworks for nine concrete cubes. Embedded studs for measuring expansion were located six inches apart and two inches away from each edge, as shown **Figure 3-6 (a)**. The detachable formworks were used to cast the nine cubes needed for expansion and DRI testing. Four expansion

measuring studs were placed in each of the three perpendicular faces. **Figure 3-6 (b)** below provides a better understanding of the location and the number of studs used. Depending on the intended restraint (e.g., unrestrained, uniaxial, biaxial), four ½-inch diameter holes were drilled through the formwork walls to attach sheaths, through which the post-tensioning rods were later placed in either one or two directions. The forms were sprayed with a release agent and then concrete placed and consolidated into the form in three equal lifts. Finally, the concrete was cured for 24 hours before the forms were removed.

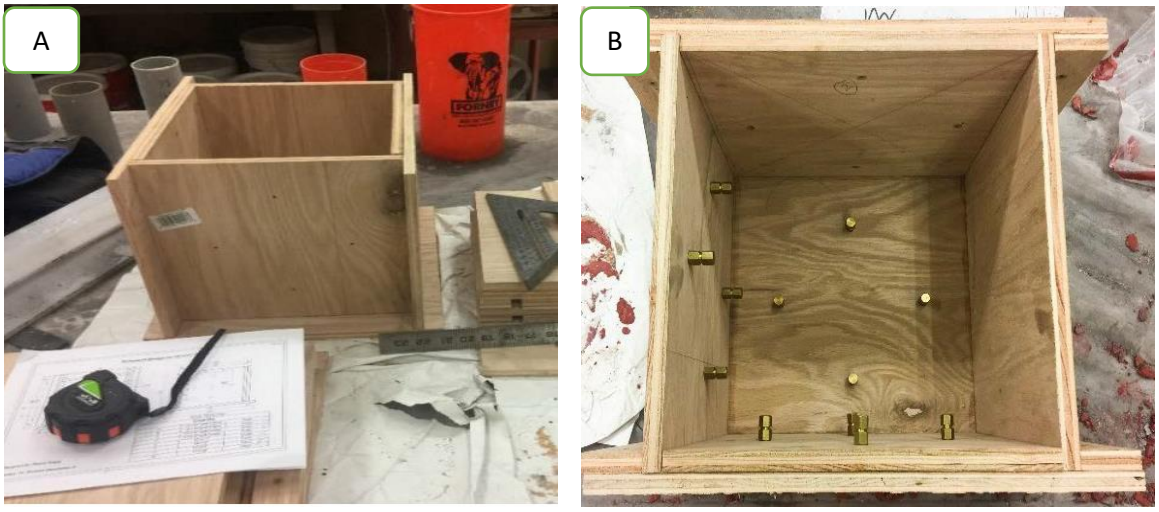

Figure 3-6, (a) A cubic ten-inch formwork. (b) Embedded expansion studs (pictures by Romit Thapa)

To monitor expansion, a 0.001 inch-resolution detachable mechanical length-change gauge, shown in **Figure 3-7** was used to periodically measure length change over a two-year period. The gauge was zeroed with a 6 inch long, Invar reference bar before any length-change measurement were taken. The strain was calculated by dividing the length-change (the gauge reading after zeroing with the 6-inch reference bar) by the initial length of 6 inches.

Figure 3-7, Detachable mechanical gauge (picture by Romit Thapa)

Before placing the concrete, 9.5-inch stainless steel tubes with an inside diameter of 0.70 in and a wall thickness of 0.08 in were placed into the forms as shown in **Figure 3-8**. The sheaths were 0.5 inches shorter than the cube to prevent any stress transfer into the sheaths. The sheaths were required to place post-tensioning rods after casting. The inside diameter of the sheaths was chosen slightly larger than the diameter of the post-tensioning rods to guarantee the free movement of rods, thereby limiting stress transfer to the cube surface. Four sheaths were located along each restrained axis. **Figure 3-8** shows how the tubes were located in both uniaxially and biaxially restrained cubes. Finally, the sheaths were coated with a release agent to prevent bond with the concrete.

Figure 3-8, Expansion test cubes formworks (a) Uniaxially restraint cube formwork with sheaths installed (b) Biaxially restraint cube formwork for with sheaths installed. (pictures by Romit Thapa)

Ductile, high-strength Class 10M threaded rods and nuts were used to post-tension the cubes along the restrained axes. Class 10M has a similar thermal expansion coefficient to that of the concrete used in this test. Class 10M hex nuts were used to tighten the bolts. Also, high strength carbon steel plates (ASTM 1018) were used with the bolts to distribute the stresses over the face of the cube. The dimensions of the plates were 3 x 3 x ½ in with a 0.60 in hole drilled in the center of each plate for the bolts. The Class 10M rods have a yield strength of 130 ksi and a tensile strength of 145 ksi. The carbon steel plates have a yield strength of 55 ksi and a tensile strength of 65 ksi. **Figure 3-9** shows the bolts, plates, and nuts after demolding and tensioning.

Figure 3-9, uniaxial restraint cube after demolding and tightening the bolts (stress is applied) (picture by Romit Thapa)

3.4.3 Casting, Conditioning and Loading of Specimens

As previously mentioned, the mix design (**Table 3-3**) was used to cast nine cube specimens. Concrete from the same batch was used to cast 4x8 in cylindrical specimens for compressive strength test and modulus of elasticity test at 28 day-age. Cement, water, fine aggregate, and coarse aggregate were weighted and prepared for mixing, as shown in **Figure 3-10**.

Figure 3-10, Preparation of mix design before batching. (picture by Romit Thapa)

The NaOH pellets were added and dissolved into the mixing water to achieve a Na_2O_e content of 1.25 percent. Mixing and casting were done in the concrete lab at

Youngstown State University, with a controlled temperature of 22 ºC. The inner surfaces of the nine formworks were sprayed with WD-40 to ease the demolding process. Concrete was placed in formworks in three layers. Each layer was rodded 25 times. The third (top) layer was troweled to produce an even smooth surface. At the same time, cylindrical plastic molds were sprayed with WD-40 before casting cylinders for compression and modulus of elasticity tests.

After casting, all test specimens were stored in the concrete lab at the room temperature (22 º C) before demolding. Specimens were demolded 24 hours after casting and cured at 95-100 percent RH (not in contact with water) for 56 days. The purpose of this process was to provide moisture without alkalis being leached from the concrete. After curing, specimens were moved to a chamber with a temperature between 97 º F and 104 º F and the RH greater than 95%. **Figure 3-11** shows the specimens stored in the chamber.

Figure 3-11, Specimens in the chamber where RH is more than 95% and temperature is 38 ± 2º C. (picture by Romit Thapa)

At an age of 56 days, the post-tensioning rods were tightened to produce the desired confining stresses. The nine cubes were divided into three subsets, each group with a

different stress state. The first three cubes were unrestrained, so no external stress was applied on those three cubes. The second set of cubes was uniaxially restrained, with the post-tensioning along the X-axis tightened to provide a confining stress of 5 MPa (725 psi). For the biaxial restrained set, the post-tensioning was tightened to produce stresses of 5 MPa (725 psi) and 4 MPa (580 psi) along the X-axis and the Y-axis, respectively.

3.4.4 Test Details

Before placing the cube specimens in the environmental chamber, initial strain was recorded along each perpendicular axis of each of the nine cube specimens. After this, strain was measured bi-weekly, and the data recorded. The specimens were stored in the environmental chamber except when taking measurements. Before measuring strain, the cubes were cooled to 21 °C over a period of 16-24 hours to minimize errors caused by thermal strain. Upon reaching an average strain of 0.15, 0.25, and 0.35 percent (in the unrestrained direction) one cube from each subset (unrestrained, uniaxial, biaxial) were removed from the experiment for DRI testing (a destructive test method). The three strain values were reaches at ages of 97, 152 and 416 days, respectively.

3.5 DRI Test

One cube of each set was prepared for DRI testing when the required average strain was reached at the ages of 97 days (~3 ½ months), 274 days (~5 months) and 472 days (~ 14 months), respectively. Cubes were labeled using a right-handed coordinate system, as shown in **Figure 3-12**. Each 10 × 10 in cube was cut into eight 5 × 5 in cubes using a diamond wet saw (**Figure 3-13**). Only four reasonably intact sub-cubes were selected from each cube for DRI testing. Only four sub-cubes were required to provide a surface area of

200 cm^2 in each plane (X, Y, Z). The remaining cubes were stored at room temperature for further evaluation if required.

Figure 3-12, Cubes were labeled before they were cut to 5 × 5 in cubes (pictures by Ali Qutail)

Figure 3-13, The electrical blade used to cut the cubic specimens (pictures by Ali Qutail)

Samples were cut and carefully polished using a hand-polisher. A grid of 1 cm^2 cells was drawn on the concrete surface. After sample preparation, a 15-16x magnification

stereomicroscope was used to analyze each 1 cm^2 cell on the concrete surface. Each deterioration feature is multiplied by a weighing factor. The final DRI is the summation of all features on the surface normalized to a 100 cm^2 surface area (typically an area of 200 cm^2 is analyzed to reduce error). The weighing factors for ASR features are summarized in **Table 2-3**.

In this thesis an average modified DRI (M-DRI) was calculated, as only four of the deterioration features were found to be affected primarily by the confining stress states: open cracks in aggregate with and without gel (OCAG and OCA) and cracks in cement paste with and without gel (CCPG and CCP). The average M-DRI was calculated as the summation of only these four deterioration features. The remaining features (CCA, DAP, CAD) occur independent of confinement.

4 Results and Discussion

The reactivity of The Jobe-Newman sand (from El Paso, TX) and non-reactive sand (from Youngstown, OH) was tested in accordance with ASTM 1260 (AMBT). Also, the expansion of concrete prisms was monitored in accordance with ASTM C1239 (CPT). In addition, the compressive test and the modulus of elasticity test were performed on cylindrical specimens in accordance with ASTM C39 and ASTM C469, respectively.

The axial expansions of the nine concrete cubes were monitored for 416 days. The nine cubes were divided equally to three subsets (three stress states) as follows: three unrestraint cubes, three uniaxially restrained cubes, and three biaxially restrained cubes. For the three unrestrained cubes, no stress was applied. For the three uniaxially restrained cubes, A stress of 5 MPa (725 psi) was applied along the X-axis. Finally, the three biaxially restrained cubes had stresses of 5 MPa (725 psi) and 4 MPa (580 psi) applied along the X-axis and the Y-axis, respectively. The expansion (strain) was measured using the embedded studs and detachable mechanical gauge (discussed in Section 3.4). The cube specimens were stored at 38 ºC and 98% RH to accelerate the rate of ASR. The strains were monitored bi-weekly throughout the duration of testing. The strain data collected were averaged and analyzed for X, Y and Z axes. Finally, three cubes (one of each stress state) were tested at three different ages following the DRI method when the average strain (unrestrained) reaches 0.15%, 0.25% and 0.35%.

4.1 AMBT (ASTM C1260)

The Jobe sand (reactive sand) and a non-reactive fine aggregate were tested for reactivity using AMBT in accordance with ASTM C1260. Mortar bars were cast for each aggregate. Initial readings and five subsequent readings were recorded over a 28-day

period. The expansion data is summarized in **Table A- 1** the expansion results for the Jobe sand mortar bars at different ages. Also, the expansion of six samples, made using non-reactive sand, was monitored and the results are summarized in **Table A- 2.** As indicated in **Figure 4-1**, the expansion at 14 days was 0.34% (underlined in **Table A- 1**) for the Jobe sand mortar bars, which is greater than the threshold of 0.10%, indicating deleterious expansion. On the other hand, the average expansion for the non-reactive sand mortar bars was 0.09% (underlined in **Table A- 2**) at 14 days, which indicates that it is a non-reactive (inert) sand.

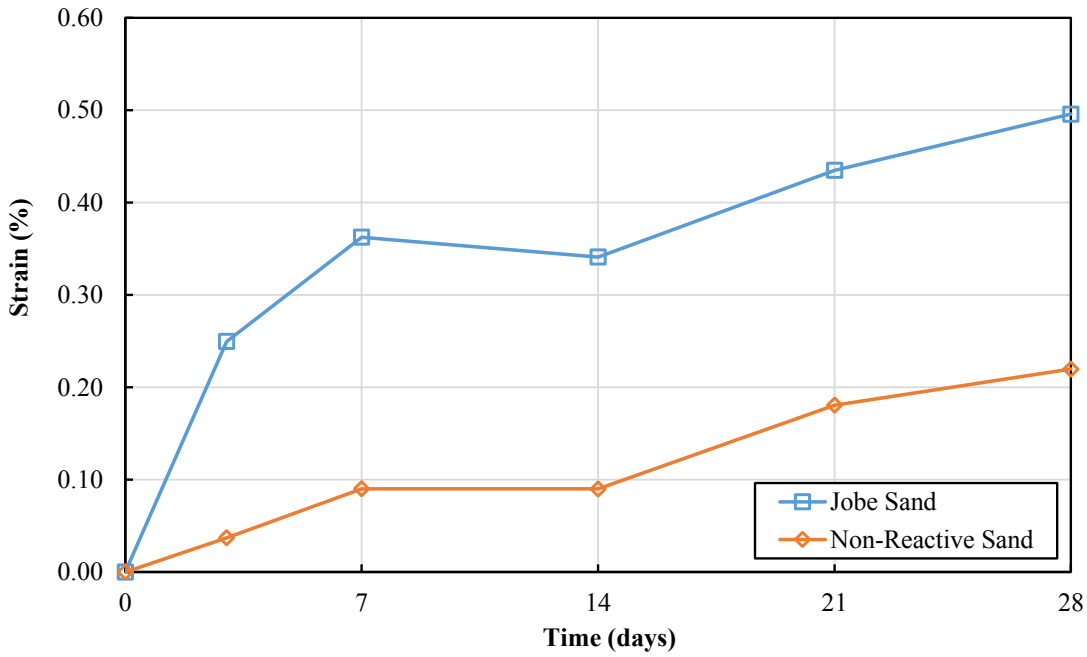

Figure 4-1, Expansions of Jobe Sand and Non-Reactive Mortar Bars (AMBT ASTM C1260)

4.2 CPT (ASTM C1293)

Concrete prisms were cast, as described in Section 3.2, in the concrete lab to monitor strain in accordance with ASTM C1293. The expansion results of the six samples at

different ages are summarized in **Table A- 3**. The average strain at each age was calculated and plotted. The expansion rate was high during the first 68 days, and then slowed after it exceeded a strain value of 0.26%, as shown in **Figure 4-2**, below. The expansion exceeded the CPT threshold of 0.04% within 12 days, indicating deleterious expansion.

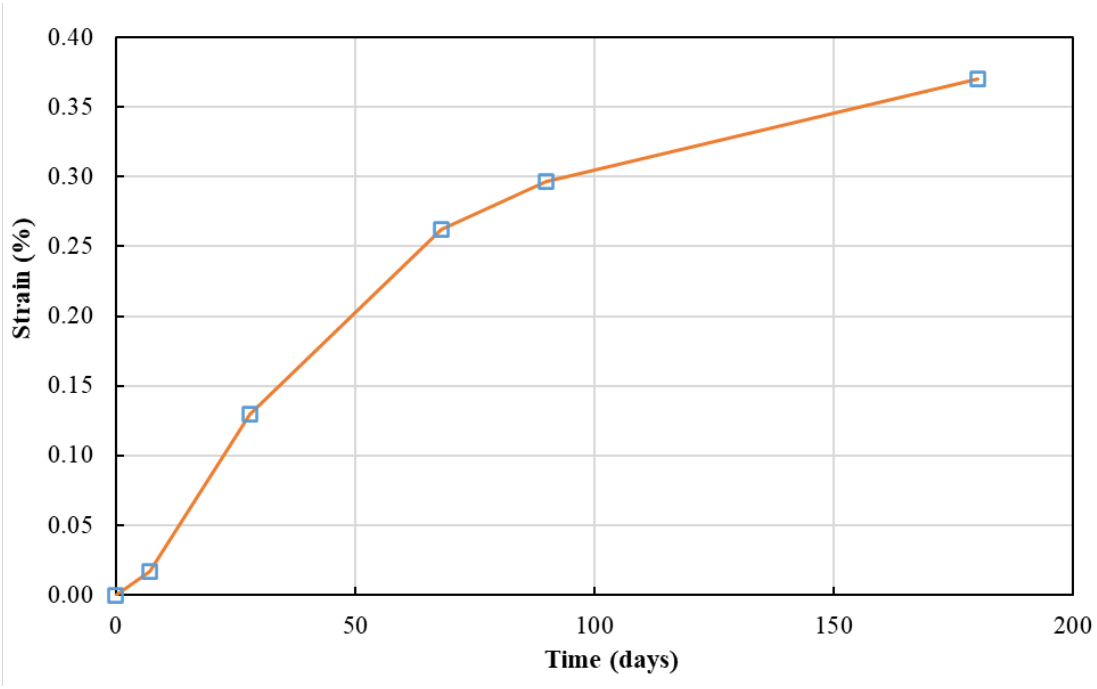

Figure 4-2, CPT Results (ASTM C1293)

4.3 Compressive Strength Test and Modulus of Elasticity Test

The compressive test (ASTM C39) and the modulus of elasticity test (ASTM C469) were performed on cylindrical specimens. The specimens were stored at the room temperature for 28 days. Then, eight specimens were tested to determine the compressive strength. The average compressive strength of the specimens was 41.50 MPa (6020 psi). The other eight specimens were tested to determine the modulus of elasticity after they

were loaded to 40% of the ultimate compressive strength (around 17 MPa [2466 psi]). The average modulus of elasticity was 30.90 GPa (4480 ksi).

4.4 Cube Expansion Test

The first subset of cubes consisted of three unrestrained cubes, which will be referred to as B1C1, B1C2 and B1C3. The first cube (B1C1) was removed from the environmental chamber after 96 days when the average strain reached 0.15%. The second cube (B1C2) and the third cube (B1C3) were taken out after 218 and 416 days when the average strain values exceeded 0.25% and 0.35%, respectively.

Table A- 4 summarizes the average axial strain values between the day of the initial reading and the 97th day for the B1C1-named cube. Also, **Table A- 5** and **Table A- 6** show the axial average strain data for B1C2 and B1C3-named cubes, respectively.

The second subset of cubes consisted of three cubes cast for the uniaxial confinement, which were labeled B2C1, B2C2 and B2C3. A confining stress of 5.0 MPa (725 psi) was applied along the X-axis of each cube. B2C1 was taken out of the chamber after 96 days. B2C2 and B2C3 were taken out after 218 and 416 days, respectively. **Table A- 7**, **Table A- 8** and **Table A- 9** summarize the expansion data for the three uniaxially restraint cubes.

Finally, the third subset of three cubes was cast for the biaxial confinement and labeled B3C1, B3C2 and B3C3. A confining stress of 4.0 MPa (580 psi) was applied along the Y-axis of each cube. and a confining stress of 5.0 MPa (725 psi) was applied along the X-axis of each cube, as well. B3C1, B3C2 and B3C3 were taken out of the chamber after

96, 218 and 416 days, respectively. **Table A- 10, Table A- 11**, and **Table A- 12** show the expansion values of the three biaxially restrained cubes.

The average axial strain was calculated for each stress state. Between day 0 and day 97, the average strain was calculated using three cubes for each restraint type (unrestrained, uniaxial, biaxial). When cubes were removed from the experiment for DRI measurements, the strain was calculated from the remaining two, and then one cubes from each set after 96 and 218 day-age, respectively. As the DRI test is a destructive test method, the number of cubes remaining in each subset decreased to two and then one after 96 and 218 days, respectively. **Table A- 13**, **Table A- 14** and **Table A- 15** summarize the average axial strain for unrestrained, uniaxially restrained, and biaxially restrained cubes, respectively.

The average strain increased at similar rates along all three axes in the unrestrained cubes. The expansion rate was higher during the first 100 days but decreased over the time, comparable to the trend observed in the ASTM C1293 testing. The maximum average strain (reached at 416 days) was comparable along all three axes. The strain ranged between 0.4267% and 0.5058%. Also, the average strain values remained similar throughout monitoring. **Figure 4-3** shows the average strain values for the unrestrained cubes during the 416 days of monitoring. Similarly, **Figure 4-4** and **Figure 4-5** show the average strain values for the uniaxially and biaxially restrained cubes, respectively. In the uniaxially restrained cubes, the strain values were lesser along the restrained axis (X-axis). The strain values along the unrestrained axes (Y-axis and Z-axis) were comparable to those recorded in the first set of cubes (unrestrained cubes). The maximum average strain along the X-axis was 0.2263%, Which is approximately half of the strain along the X-axis in the unrestrained cubes (0.4267%). In the biaxially restrained cubes, the strain values were

lesser along both restrained axes as compared to the unrestrained axis. Along the X-axis, the average strain at 416 days was 0.0583%, which is approximately 11% of the average strain at the same point in the unrestrained cubes. Similarly, the average strain along the Y-axis was lower than that of the X-axis because the confining stress was only 4 MPa (145 psi). The average strain along the Y-axis at 416 days was 0.1367%, lower than the strain along the why axis in the restrained cubes by 73%. **Table 4-1** and **Figure 4-6** summarize the average axial strain at 416 days for all three stress states.

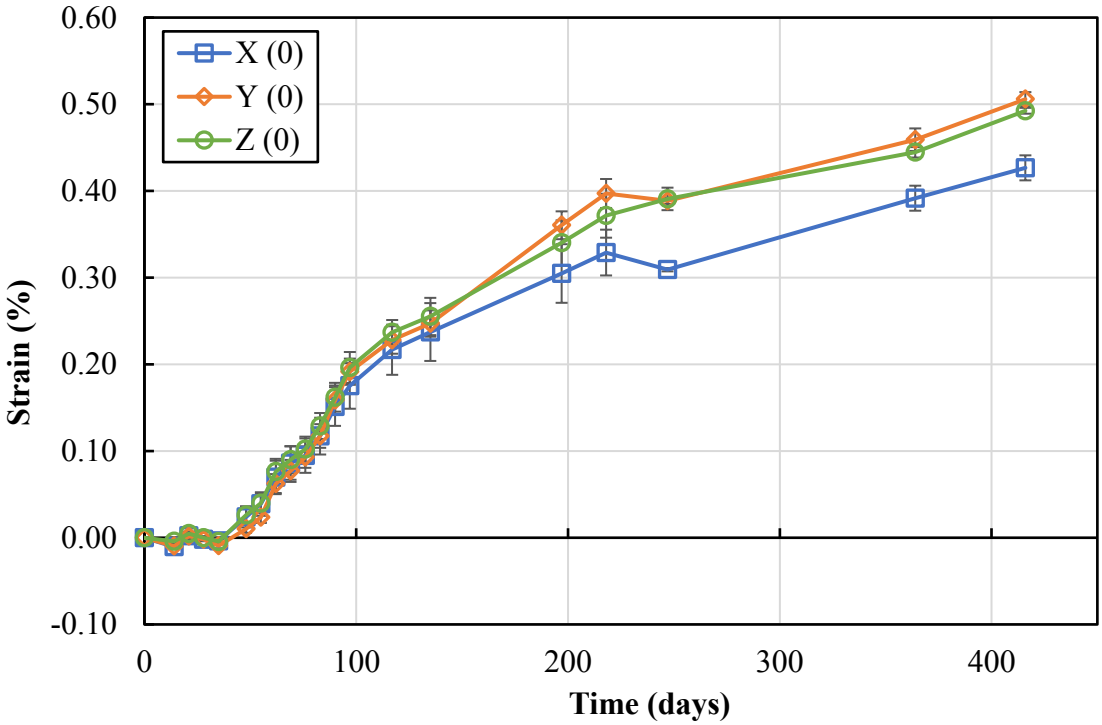

Figure 4-3, Avg. Strain for Unrestrained Cubes Over 416 Days

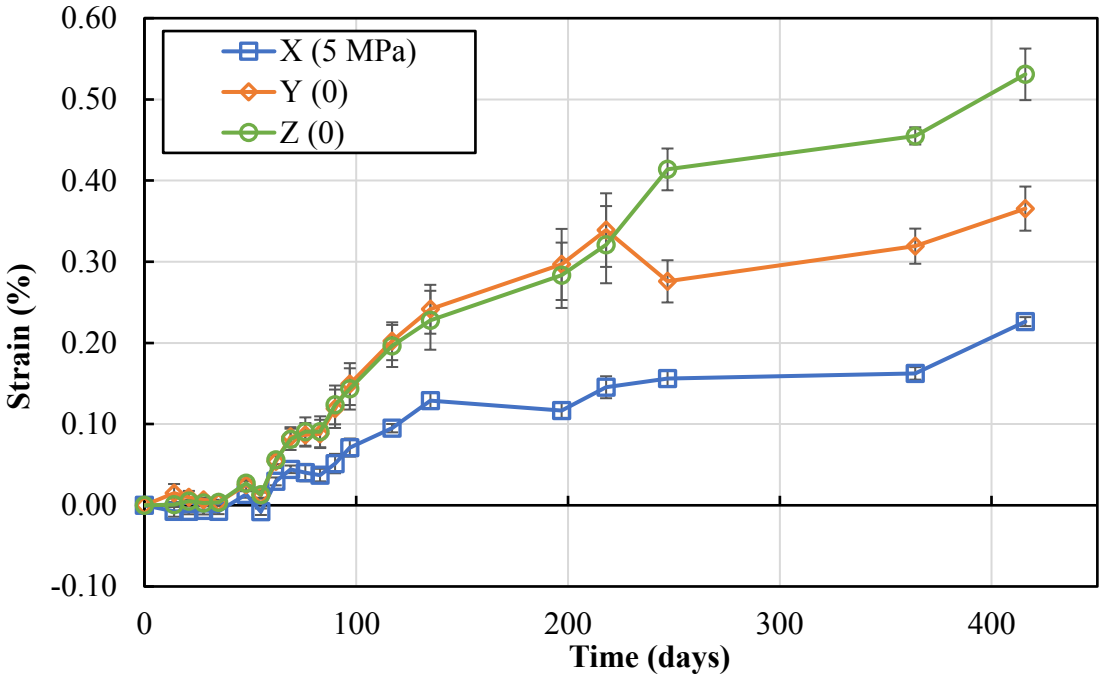

Figure 4-4, Avg. Strain for Uniaxially Restrained Cubes Over 416 Days

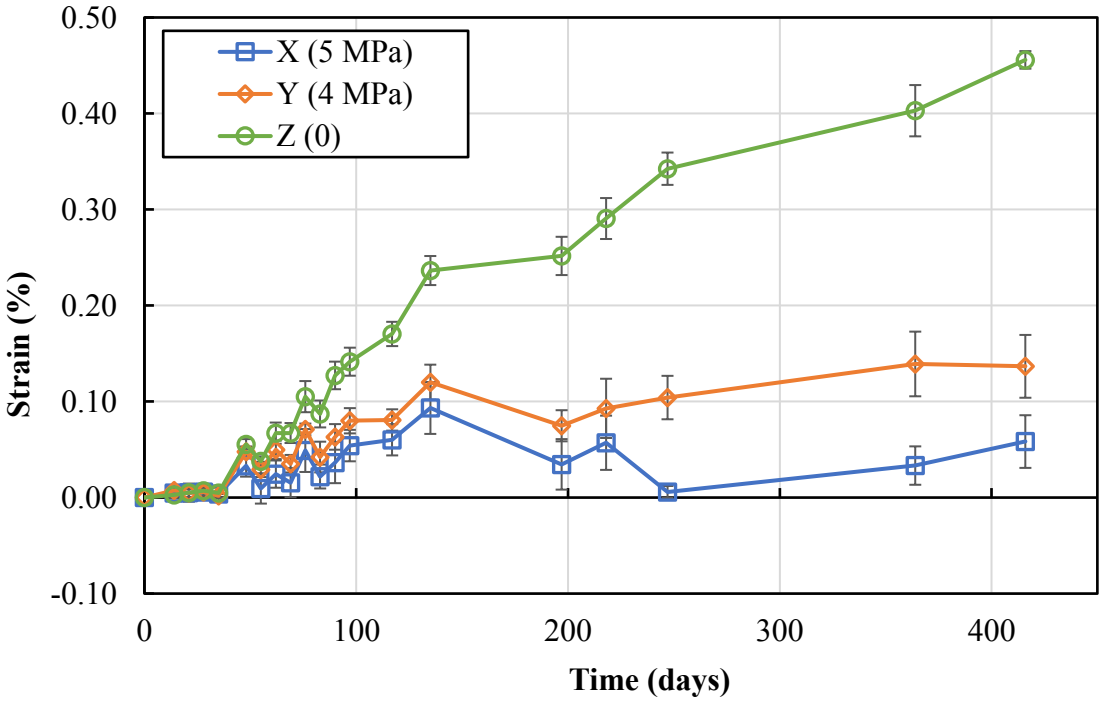

Figure 4-5, Avg. Strain for Biaxially Restrained Cubes Over 416 Days

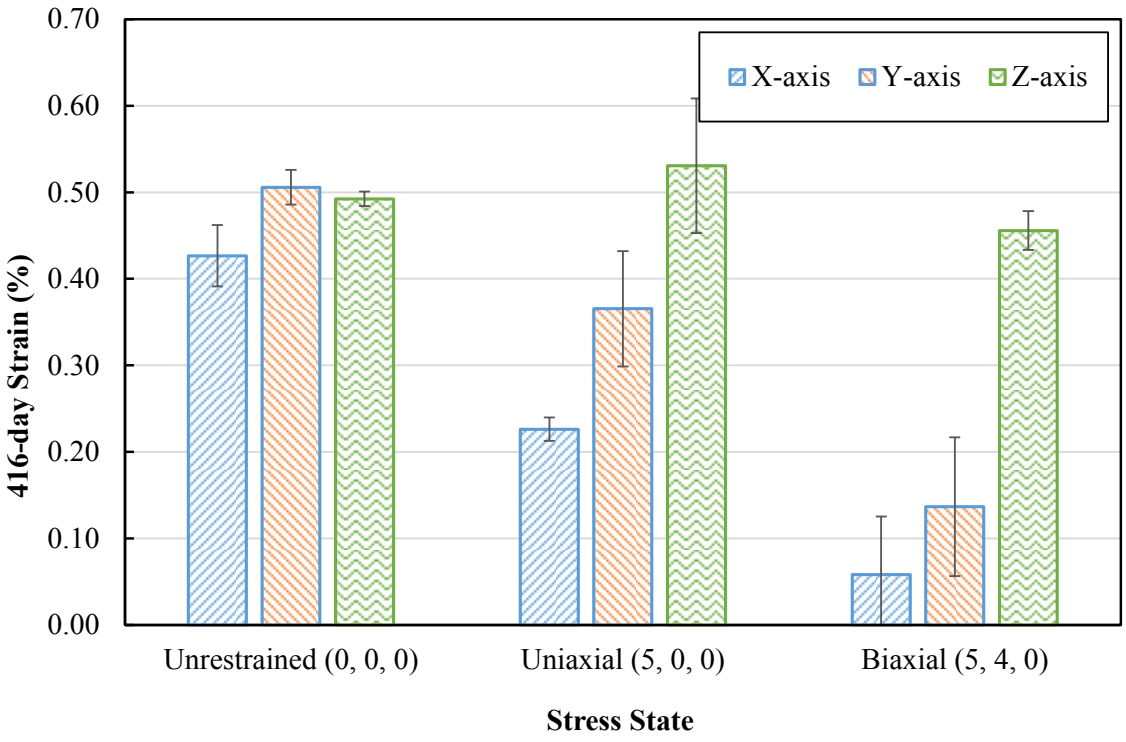

Figure 4-6, Axially Avg. Strain at 416 Days for All Three Stress States

As shown in **Figure 4-6** above, the axial strain along the restrained axis/axes (X-axis in the uniaxially restrained cubes, and X-axis and Y-axis in the biaxially restrained cubes) was considerably less than the strain along the same axis/axes when it/they were not restrained. The strain in along the X-axis in the first set of cubes (unrestrained cubes) was 0.43%, but it decreased to be 0.22% and 0.05% in the uniaxially and biaxially restrained cubes, respectively. Also, the strain along the Y-axis was lower. The strain along the Y-axis was 0.51% when it was not restrained, and it decreases to 0.13% when it was restrained by a 4 MPa stress. This further decrease in strain in the Y and Z axes for the biaxially restrained specimen indicates the confining stress in these planes reduced the expansion in perpendicular planes.

Table 4-1, Axially Avg. Strain at 416 Days for All Three Stress States.

Stress State	X-axis maximum strain (%)	Y-axis maximum strain (%)	Z-axis maximum strain (%)
Unrestrained Cubes	0.4267	0.5058	0.4925
Uniaxial Cubes	0.2263	0.3654	0.5308
Biaxial Cubes	0.0583	0.1367	0.4558

The volumetric strain (the sum of strains along all three axes), was also calculated at all ages for the three stress states, with the results are summarized in **Table A- 16**. The volumetric strain in the unrestrained cubes was the highest at any age with a maximum of 1.425% at 416 days. In the uniaxially restrained cubes, the volumetric strain was always higher than that of the biaxially cubes and lower than that of the unrestrained cubes. The maximum volumetric strain (at 416 days) strain was 1.1225% and 0.06508% in the uniaxially restrained cubes and the biaxially restrained cubes, respectively. **Figure 4-7** shows the volumetric strain for all three stress states over the 416 days monitoring period. The restraints were effective to reduce ASR expansion in all cases. The volumetric strain in the biaxially restrained cubes was always less than the volumetric strain in the uniaxially restrained cubes. Also, the volumetric strain in the uniaxially restrained cubes was always less than the volumetric strain in the unrestrained cubes. The volumetric strain at 416 days in the unrestrained cubes was 1.425%, but in the case of uniaxially restrained and biaxially restrained cubes, the volumetric strain was 1.2225% and 0.6508%. The volumetric strain was reduced by 14% in the uniaxially restrained cubes. It was also reduced by 54% in the biaxially restrained cubes, as shown in **Figure 4-7**.

The axial strain along the X-axis and the Y-axis in the biaxially restrained cubes (**Figure 4-5**) decreased between 100 and 200 days, which is thought to have occurred due

to crack formation and slippage in the unrestrained direction (Z-axis), which indicated an increase in strain over around 200 days. That was also noticeable when the volumetric strain for the biaxially restrained cubes was determined (**Figure 4-7**).

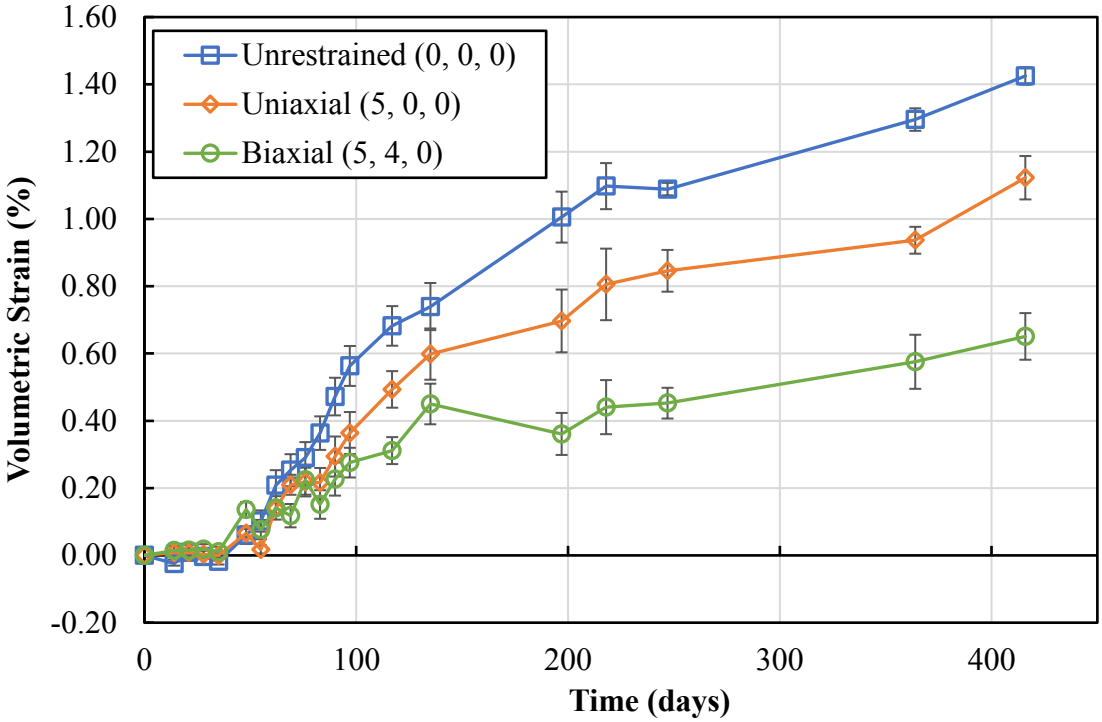

Figure 4-7, Volumetric Strain for All Three Stress States

4.5 DRI Test

At 97 days of exposure (when an average of 0.15% strain was reached), the cubes B1C1, B2C1 and B3C1 were moved out of the chamber and prepared for DRI testing. Later, at 152 days of exposure (when an average of 0.25% strain was reached), B1C2, B2C2 and B3C2 were moved and prepared for DRI test. Finally, B1C3, B2C3 and B3C3 were moved and prepared for the DRI test at 416 day-age (when an average of 0.35% strain was reached). An average modified DRI (M-DRI) was calculated as the summation of the count of four types of cracks: open cracks in aggregate with and without gel (OCAG and

OCA) and cracks in cement paste with and without gel (CCPG and CCP). The modified DRI is suggested herein as the restraint (stress state) primarily affect the formation of these four deterioration features to a greater degree than the other features. **Table 4-2** shows the average M-DRI values for the unrestrained cubes.

Table 4-2, Average M-DRI Values for Unrestrained Cubes.

Plane	Age (Days)	Crack Type				Modified DRI Value
		OCA	OCAG	CCP	CCPG	
B1C1 X(0)	**97**	72	0	142	4	**218**
B1C1 Y(0)		79	2	212	11	**302**
B1C1 Z(0)		86	1	188	5	**279**
B1C2 X(0)	**152**	11	5	194	12	**218**
B1C2 Y(0)		10	1	253	1	**265**
B1C2 Z(0)		17	0	346	0	**363**
B1C3 X(0)	**416**	11	0	292	0	**303**
B1C3 Y(0)		5	0	259	0	**264**
B1C3 Z(0)		14	0	282	0	**296**

It is apparent that the average M-DRI values for the unrestrained cubes (at each age) are similar since none of the perpendicular planes were subjected to any confining stresses. This allowed the cracks to propagate in all directions randomly. At 97-day age, the M-DRI ranged between 218 and 308 and the average M-DRI was 266. At 152-day age, it ranged between 218 and 363 and the average was 282. At 416-day age, it ranged between 264 and 303 and the average was 287. The average M-DRI values did not increase with age. Of note, the DRI measured at 97-days was counted by a different operator than those measured at 152 and 416 days, which may introduce some bias into the results as inter-operator error for the DRI test method is up to 40% (Villeneuve and Fournier, 2012)

Table 4-3 summarizes the average M-DRI values for all uniaxially restrained cubes. The average M-DRI value was 60, 144 and 301 at 97, 152 and 416 day-age, respectively. A noticeable increase of the average M-DRI values was recorded with expansion (age). At 97 and 416 day-age, the highest average M-DRI values were recorded on X-face (plane normal to the X axis). That result was expected as the stress of 5 MPa (725 psi) was applied along the X-axis which leaves the X plane (Y and Z axes) with less restraint but inhibits cracking on the other two planes (Y and Z). Hence, the cracks propagated more on the X face, which leads to a higher average M-DRI value.

Table 4-3, Average M-DRI Values for Uniaxially Restrained Cubes.

Plane	Age (Days)	Crack Type				Modified DRI Value
		OCA	OCAG	CCP	CCPG	
B2C1 X (5 MPa)	**97**	47	0	26	1	**74**
B2C1 Y (0)		31	0	16	1	**48**
B2C1 Z (0)		34	0	25	0	**59**
B2C3 X (5 MPa)	**152**	4	0	146	0	**150**
B2C2 Y (0)		11	0	106	0	**117**
B2C2 Z (0)		8	0	156	0	**164***
B2C3 X (5 MPa)	**416**	18	0	414	0	**432**
B2C3 Y (0)		10	0	319	0	**330**
B2C3 Z (0)		10	0	131	0	**141**

***** It is expected that the M-DRI for the Y-face and Z-face should be lower due to restraint. The average M-DRI at 152 days did not match the expectation. However, the expected trend was clear at 416-days when expansion was greater, and the cracks were more apparent.

Table 4-4 is a summary of the average M-DRI values for the biaxially restrained cubes. The average M-DRI also increased with the expansion (age). The average M-DRI values at 97, 152 and 416 day-age were 74, 98 and 139, respectively. At 152 and 416 day-age, the X face had the largest average M-DRI as the restraint was applied along the X and the Y axes. Also, the Z-face (plane normal to the Z axis) showed the least average M-DRI value since it had been affected by both restraint along the X and Y axes.

Table 4-4, Average M-DRI Values for Biaxially Restraint Cubes.

Plane	Age (Days)	Crack Type				Modified DRI Value
		OCA	OCAG	CCP	CCPG	
B3C1 X (5 MPa)	**97**	57	0	19	0	**76**
B3C1 Y (4 MPa)		45	0	20	0	**65**
B3C1 Z (0)		52	1	29	0	**82***
B3C2 X (5 MPa)	**152**	9	0	127	0	**137**
B3C2 Y (4 MPa)		5	0	91	0	**96**
B3C2 Z (0)		2	0	60	0	**62**
B3C3 X (5 MPa)	**416**	2	0	203	0	**205**
B3C3 Y (4 MPa)		5	0	135	0	**139**
B3C3 Z (0)		5	0	69	0	**74**

***** It is expected that the M-DRI for the Z-face should be lower due to restraint. The average M-DRI at 97 days did not match the expectation. However, the expected trend was clear at 416-days when expansion was greater, and the cracks were more apparent.

Table A- 17 is a summary of the number of each deterioration features counted in each face at three ages for unrestrained cubes. **Table A- 18** and **Table A- 19** show the same data for the uniaxially and biaxially restrained cubes, respectively. All seven deterioration features, closed cracks in aggregate (CCA), open cracks in aggregate with and without gel (OCAG and OCA), coarse aggregate de-bond (CAB), disaggregated aggregate particles (DAP), cracks in cement paste with and without gel (CCPG and CCP) were counted and summarized in **Table A- 17** through **Table A-** 19.

In Figure 4-8, The count of deterioration features in all nine cubes are summarized in a bar graph. The results indicate the same patterns mentioned for **Table 4-2**, **Table 4-3**, **Table 4-4**. Note the DRI method includes seven deterioration features, some of which are not influenced by external restraint (e.g., CCA, CAD, DAP), while the remaining features used in the average M-DRI method (OCA, OCAG, CCP, and CCPG,) are more likely to be influenced by restraint. Additionally, the DRI for the first three cubes (at 0.15% strain)

were tested by a former researcher (Thapa, 2018). It is expected to have not more than 40% variation when the DRI as counted by two different operators.

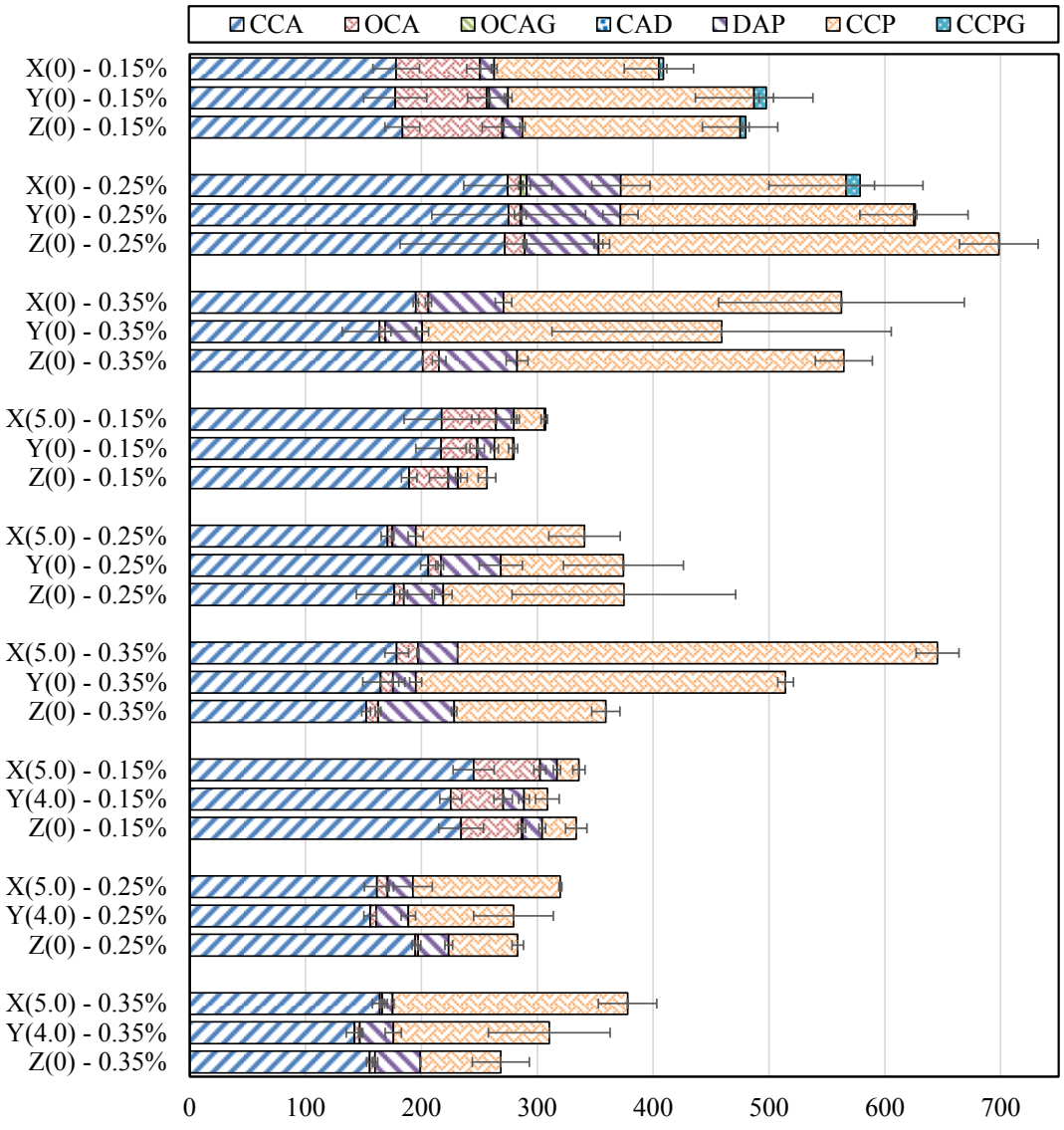

Figure 4-8, Cracks in Each Plane for the Three Stress States at the Three ages

5 Conclusion

In summary, the objective of this research was to study the effect of different stress states on the progression of ASR in concrete pavements. The expansion of nine cubes were monitored over the research period (416 day). The DRI test was also performed on the same specimens, at expansion of 0.15, 0.25, and 0.35%. The result of the expansion test and the DRI lead to the following conclusions:

(i) Confining stresses were sufficient to reduce the axial expansion along the restrained axes. In the first set of cubes (no stresses were applied), the average strain values were similar throughout the duration of monitoring along the three perpendicular axes. In the second set of cubes (uniaxially restrained 5 MPa (725 psi) along the X-axis), the expansion along the X-axis was reduced as compared to the unrestrained directions. Also, the expansion was reduced along restrained the X and Y axes in the third set of cubes (biaxially restrained 5 MPa (725 psi) and 4 MPa (580 psi) along the X-axis and Y-axis, respectively).

(ii) The applied restraint was sufficient to reduce expansion along the restrained axes. The expansion along the free axes in the uniaxially and biaxially restrained cubes was comparable to the average axial expansion in the unrestrained cubes. The results are in line with those of other experiments where uniaxial and biaxial restrained concrete with ASR expansion was evaluated (Multon, 2016, Gautam, 2017, Thapa, 2018).

(iii) Confining stresses were not sufficient to stop all ASR expansion but sufficient to reduce the volumetric expansion.

(iv) The final expansion depends on the magnitude of the applied stress. In the biaxially restrained cubes, the expansion along the X-axis (a stress of 5 MPa (725 psi) was

applied along the X-axis) was always lower than the expansion along the Y-axis (a stress of 4MPa (580 psi) was applied along the Y-axis).

(v) DRI test results indicate that the stresses are effective to reduce the degree of damage in the planes perpendicular to the restrained axes. In the uniaxially restrained cubes, The Y-plane and Z-plane have lesser average M-DRI values than the X-axis. Also, In the biaxially restrained cubes, The Z-plane has the least average M-DRI value due to the combined effect of restraint along the X and Y axes.

6 References

1. Ahmed, T., Burley, E., Rigden, S., Abu-Taira, A. I., "The Effect of Alkali Reactivity on the Mechanical Properties of Concrete.", *Construction and Building Materials*, Vol. 17, 2003, pp. 123-144.
2. Ahmed, T., Burley, E., Rigden, S., Abu-Taira, A. I., "The Effect of Alkali Reactivity on the Mechanical Properties of Concrete.", *Construction and Building Materials*, Vol. 17, 2003, pp. 123-144.
3. Allford, M.T., "Expansion Behavior of Reinforced Concrete Elements Due to Alkali-Silica Reaction.", The University of Texas, Austin, TX, 2016, 166 pg.
4. ASTM C1260. "Standard Test Method for Potential Alkali Reactivity of Aggregates (Mortar-Bar Method)." ASTM International, West Conshohocken, United States, 2001, p. 5.
5. ASTM C1293. "Standard Test Method for Determination of Length Change of Concrete Due to Alkali–Silica Reaction." West Conshohocken, PA: ASTM International, vol. 7, 2008.
6. ASTM C39. "Standard Test Method for Compressive Strength of Cylindrical Concrete Specimens." *ASTM International*, 2001.
7. ASTM C469. "Standard Test Method for Static Modulus of Elasticity and Poisson's Ratio of Concrete in Compression." *ASTM International*, 2014.
8. Batic, O.R., Sota, J.D., "Internal Deleterious Rreactions.", in: E.F. Irassar (Ed.), "Structural Concrete Durability.", Argentina, 2002, pp. 157–216.
9. Bellew, G. P.E., "Test Methodology and Criteria for Evaluating the Potential Reactivity of Aggregates.", Proc. 8th ICAAR, Kyoto Japan, 1989, pp. 279–294.

10. Berra, M., Mangialardi, T., Paolini, A.E., Rapid Evaluation of the Threshold Alkali Level for Alkali-Reactive Siliceous aggregates in Concrete.", *Cement and Concrete Composites*, Vol. 21, 1999, pp. 325-333.
11. Bérubé M.A., Duchesne J., Dorion J.F., Rivest M., "Laboratory Assessment of Alkali Contribution by Aggregates to Concrete and Application to Concrete Structures Affected by Alkali–Silica Reactivity.", *Cement Concrete, Research* 32, 2002, pp. 1215-1227.
12. Brantley, S.L., Kubicki, J.D., White, A.F., "Kinetics of Water–Rock Interaction.", Springer, New York, 2008.
13. Broekmans, M.A.T.M., "The Alkali–Silica Reaction: Mineralogical and Geochemical Aspects of Some Dutch Concretes and Norwegian Mylonites.", Ph.D. Dissertation, Utrecht University, 2002.
14. CAN/CSA-A23.2-27A-09, "Standard Practice to Identify Potential for Alkali Reactivity of Aggregates and Measures to Avoid Deleterious Expansion in Concrete.", Canadian Standards Association, 2009.
15. Cavalcanti, A.J.C.T. and Silveira, J.F.A., "Investigations on the Moxoto Powerhouse Concrete Affected by Alkali-Silica Reaction.", Proceedings of the 8th International Conference on Alkali-Aggregate Reaction in Concrete, Kyoto, Japan, Editors: K. Okada, S. Nishibayashi and M. Kawamura, 1989, pp. 797-802.
16. Collins C.L., Ideker J.H., Willis G.S., Kurtis K.E., "Examination of the Effects of LiOH, LiCl, and LiNO3 on Alkali–Silica Reaction.", *Cement Concrete Research* 34, 2004, pp. 1403-1415.

Conditioned by the Grain Size of the Reactive Aggregate.", *Cement Concrete, Research* 4, 1974, pp. 591-607.

17. D.S. Lane, "Alkali–Silica Reactivity in Virginia.", Virginia Transportation Research Council, Charlottesville, Virginia, USA, 1994.
18. Diamond S., Nishibayashi S., Kawamura M., "ASR - Another Look at Mechanisms.", Proc. 8th International Conference on Alkali–Aggregate Reaction (ICAAR), Kyoto 1989, pp. 83–94.
19. Diamond S., Thaulow N., "A Study of Expansion due to Alkali–Silica Reaction as
20. Diamond, S., "A Review of Alkali–Silica Reaction and Expansion Mechanisms.", *Cement and Concrete Research*, Vol. 6, 1976, pp. 549–560.
21. Diamond, S., "Alkali Reactions in Concrete Pore Solution Effects.", 6th International Conference on AAR in Concrete, Copenhagen, Denmark, 1983, pp. 155–166.
22. Dunant, C. F., Bentz, E. C., "The Effect of Multi-Axial Restraint on ASR-Affected Concrete.", University of Toronto, Department of Civil Engineering, Toronto, Canada, 2010.
23. Dunant, C.F., Scrivener, K.L., "Effects of Aggregate Size on Alkali–Silica Reaction Induced Expansion.", *Cement Concrete Research*, Vol 42 (6), 2012, pp. 745–751.
24. Dunbar, P.A., Grattan-Bellew, P.E., "Results of damage rating evaluation of condition of concrete from a number of structures affected by ASR, CANMET/ACI International Workshop on Alkali–Aggregate Reactions in Concrete.", Darmouth, Canada, October 1995, pp. 257–266.

25. Feng X., Thomas M.D.A., Bremner T.W., Folliard K.J., Fournier B., “Summary of FHWA, “Condition of Concrete from a Number of Structures Affected by AAR.”, 1995. Fournier, B. “Report on the Diagnosis, Prognosis, and Mitigation of Alkali-Silica Reaction in Transportation Structures.”, 2010.
26. Fournier B., Bérubé, M. A., Folliard, K. J., Thomas, Michael, “Report on the Diagnosis, Prognosis, and Mitigation of Alkali-Silica Reaction (ASR) in Transportation Structures.”, FHWA-HIF-09-004, The Transtec Group, Inc., Austin, TX, 2010.
27. Fournier, B., Berubé, M., “Alkali-aggregate reaction in concrete: a review of basic concepts and engineering implications.”, *Canadian Journal of Civil Engineering* 27, (2), 2000, pp. 167–191.
28. French, W.J., “Avoiding Concrete Aggregate Problems.”, Improving Civil Engineering Structures - Old and New, 1995, pp. 65–95.
29. Gautam, B. P., “Multiaxially Loaded Concrete Undergoing Alkali-Silica Reaction.”, University of Toronto, Toronto, Canada, 2016.
30. Gautam, B. P., Panesar, D. K., Sheikh S. A., Vecchio, F. J., “Effect of Multiaxial Stresses on Alkali-Silica Reaction Damage of Concrete.”, *ACI Materials Journal*, Title No. 114-M52, Vol. 114, No. 4, 2017.
31. Gautam, B. P., Panesar, D. K., Sheikh, S. A., Vecchio, F. J., “Multiaxial Expansion-Stress Relationship for Alkali Silica Reaction-Affected Concrete.”, *ACI Materials Journal*, Title No. 114-M17, Vol. 114, No. 1, 2017.
32. Geology, T.R. West. “Applied to Engineering.” Prentice Hall, Englewood Cliffs, New Jersey, 1995.

33. Giaccio, G., Zerbino, R., Ponce, J.M., Batic, O.R., "Mechanical Behavior of Concretes Damaged by Alkali-Silica Reaction." *Cement and Concrete Research*, Vol. 38, 2008, pp. 993-1004.
34. Glasser L. S. D., Kataoka N., "The Chemistry of Alkali-Aggregate Reaction.", *Cement Concrete Research* 11, 1981, pp. 1-9.
35. Grattan-Bellew, P. E., and Mitchell L. D., "Quantitative Petrographic Analysis of Concrete - the Damage Rating Index (DRI) Method.", a Review. Proc. Marc-André Bérubé Symposium on AAR in Concrete, CANMET/ACI Advances in Concrete Technology Seminar, Montréal, Canada, 2006, pp. 321–324.
36. Hansen W., "Drying Shrinkage Mechanisms in Portland Cement Paste.", *Journal of American Ceramic Society* 70, 1987, pp. 323-328.
37. Hobbs D.W., Gutteridge W.A., "Particle Size of Aggregate and its Influence Upon the Expansion Caused by the Alkali-Silica Reaction.", *Magazine of Concrete Research* 31, 1979, pp. 235-242.
38. Hobbs, D.W., "Alkali–Silica Reaction in Concrete.", Thomas Telford, London, 1988.
39. Hou X., Struble L.J., Kirkpatrick R.J., "Formation of ASR Gel and the Role of C–S–H and Portlandite.", *Cement Concrete, Research* 34, 2004, pp. 1683-1696.
40. Jin, W., Meyer, C., Baxter, S., "Glascrete-Concrete with Glass Aggregate.", *ACI Material Journal* 97 (2), 2000, pp. 208–213.
41. Kagimoto, H. et al., "ASR Expansion, Expansive Pressure and Cracking in Concrete Prisms under Various Degrees of Restraint.". *Cement and Concrete, Research* 59, 2014, pp. 1-15.

42. Kawamura, M., Kayyali, O.A., Haque, M.N., “Effects of a fly ash on pore solution composition in calcium and sodium chloride-bearing mortars.”, *Cement Concrete Research* 18, 1988, pp. 763–773.
43. Kollek J.J., Varma S.P., Zaris C., “Measurement of OH-Concentrations of Pore Fluid Sand Expansion due to Alkali–Silica Reaction in Composite Cement Mortars.”, Proc. 8th Int. Cong. on the Chemistry of Cement, Rio de Janeiro, V.3 1986, pp. 183-189.
44. Maraghechi, H., Shafaatian, S., Fischer, G., Rajabipour, F. “The Role of Residual Cracks on Alkali Silica Reactivity of Recycled Glass Aggregates.”, *Cement and Concrete* Vol 34, 2012, pp. 41–47.
45. Marzouk, H., and S. Langdon. “The Effect of Alkali-Aggregate Reactivity on the Mechanical Properties of High and Normal Strength Concrete.” *Cement and Concrete Composites*, vol. 25, no. 4–5, 2003, pp. 549–56.
46. McConnell, D., Meilenz, R., Holland, W., Greene K.T., “Cement-Aggregate Reaction in Concrete, *ACI Journal*, Proc. 44 (10), 1947, pp. 93–128.
47. Mehta, P., Monteiro, P.J.M., “Concrete: Microstructure, Properties, and Materials.”, 3rd edition, McGraw-Hill, New York, 2005.
48. Molchanov V.S., Prikhidko N.E., “Corrosion of Silicate Glasses by Alkaline Solutions.”, Russ. Chem. Bull. 6 (10), 1957, pp. 1179-1184.
49. Moundoungou I., Bulteel D., Garcia-Diaz E., Thiéry V., Dégrugilliers P., Hammerschlag J.G., “Reduction of ASR Expansion in Concretes Based on Reactive Chert Aggregates: Effect of Alkali Neutralization capacity.”, *Construction Building Materials*, 54, 2014, pp. 147-162.

50. Multon S., Sellier A., Cyr M., “Chemo-Mechanical Modeling for Prediction of Alkali Silica Reaction (ASR) Expansion.”, *Cement Concrete Research* 39 (6), 2009, pp. 490-500.

51. Multon, S., Leklou, N., Petit, L., “Coupled Effects of Aggregate Size and Alkali Content on ASR Expansion.”, *Cement Concrete Research* Vol. 38 (3), 2008, pp. 350–359.

52. Multon, S., Sellier A., Cyr, M., “Chemo–Mechanical Modeling for Prediction of Alkali Silica Reaction (ASR) Expansion.”, *Cement and Concrete Research*, Vol. 39, 2009, pp. 490-500.

53. Multon, S., Toutlemonde F. O., “Effect of Applied Stresses on Alkali–Silica Reaction-Induced Expansions.”, *Cement and Concrete Research*, Vol. 36, 2006, pp. 912-920.

54. Peterson, K., Gress, D., Dam, T.V., Sutter, L., “Crystallized Alkali-Silica Gel in Concrete from the late 1890s.”, *Cement and Concrete Research*, Vol. 36, 2006, pp. 1523-1532.

55. Poole A.B., “Introduction to Alkali–Aggregate Reaction in Concrete.”, in: R.N. Swamy (Ed.), The Alkali Silica Reaction in Concrete, Van Nostrand Reinhold, New York,1992.

56. Poyet, S., Sellier A., Capra B., Foray G., Torrenti J.M., Cognon H., Bourdarot E., Chemical Modelling of Alkali Silica Reaction: Influence of the Reactive Aggregate Size Distribution.”, *Material Structure* 40 (2), 2007, pp. 229–239.

57. Rajabipour , F., Giannini, E., Dunant, C., Ideker , J. H., Thomas, M. D.A., “Alkali-Silica Reaction: Current Understanding of the Reaction Mechanisms and the Knowledge Gaps.”, Cement and Concrete Research, Vol. 76, 2015, pp. 130-146. Research on the Effect of LiNO3 on Alkali–Silica Reaction in New Concrete.”, *Cement Concrete Research* 40, 2010, pp. 636-642.
58. Rivard, P., and Ballivy, G., "Assesment of the Expansion Related to Alkali-Silica Reaction by the Damage Rating Index Method.", *Construction and Building Materials*, V. 19, No. 2, 2005, pp. 83-90.
59. Rivard, P., Bérubé, M.A., Ollivier, J-P., Ballivy, G., “Decrease of Pore Solution Alkalinity in Concrete Tested for Alkali–Silica Reaction.”, *Material Structure* 40, 2007, pp. 909–921.
60. Rivard, P., Bérubé, M.A., Ollivier, J-P., Ballivy, G., “Decrease of pore solution alkalinity in concrete tested for alkali–silica reaction.”, *Material Structure* 40, 2007, pp. 909–921.
61. Rivard, Patrice, François Saint-Pierre. “Assessing Alkali-Silica Reaction Damage to Concrete with Non-Destructive Methods: From the Lab to the Field.”, *Construction and Building Materials*, vol. 23, no. 2, 2009, pp. 902–909.
62. Sakaguchi Y., Takakura M., Kitagawa A., Takahiro H., Fuminori T., “The Inhibiting Effect of Lithium Compounds on Alkali–Silica Reaction, Proceeding of the 8th International Conference on Alkali–Aggregate Reaction.”, Kyoto 1989, pp. 229-234.

63. Sanchez, L.F.M., Contribution to the Assessment of Damage in Aging Concrete Infrastructures Affected by Alkali–Aggregate Reaction.", PhD thesis, Department of Geology and Geological Engineering, Université Laval, Québec, Canada, 2014.
64. Sanchez, L.F.M., Drimalas, T., Fournier, B., "Assessing condition of concrete affected by internal swelling reactions (ISR) through the Damage Rating Index (DRI).", *Cement*, 1-2, 2020, 18 pg.
65. Sanchez, L.F.M., Fournier, B., Jolinb M., Duchesne, J., "Reliable Quantification of AAR Damage Through Assessment of the Damage Rating Index (DRI).", *Concrete and Cement Research*, Vol. 67, 2015, pp. 74-92.
66. Shao Y., Lefort T., Moras S., Rodriguez D., "Studies on Concrete Containing Ground Waste Glass.", *Cement Concrete, Research* 30, 2000, pp. 91-100.
67. Shehata, M. H., Thomas, M. D.A., "The Effect of Fly Ash Composition on the Expansion of Concrete Due to Alkali-Silica Reaction.", *Cement and Concrete Research*, Vol. 30, 2000, pp. 1063-1072.
68. Shehata, M., Thomas, M.D.A., "Alkali release characteristics of blended cements.", *Cement Concrete Research*, 36, 2006, pp. 1166–1175.
69. Shon, C. S., Zollinger, D. G., Sarkar, S. L., "Evaluation of Modified ASTM C 1260 Accelerated Mortar Bar Test for Alkali-Silica Reactivity.", *Cement and Concrete Research*, Vol. 32, 2002, pp. 1981-1987.
70. Smaouia, N., Be´rube, M.A., Fournierc, B., Bissonnetted, B., Durande, B., "Effects of Alkali Addition on the Mechanical Properties and Durability of Concrete.", *Cement and Concrete Research*, Vol. 35, 2005, pp. 203-212.

71. Stanton, T.E., “Expansion of Concrete through Reaction between Cement and Aggregate.”, Proc. Am. Soc. Civ. Eng. 66 (10), 1940, pp. 1781–1811.
72. Stark D.C., “Lithium Salt Admixtures - An Alternative Method to Prevent Excessive Alkali–Silica Reactivity.”, 9th ICAAR, International Conference on Alkali Aggregate Reactions, London, 1992.
73. Swamy, R. N., Al-Asali M. M., “Engineering Properties of Concrete Affected by Alkali-Silica Reaction.”, *ACI Materials Journal*, vol. 85, no. 5, 1988, pp. 367-374.
74. Takahashi, Y., Segawa, I., Gong, F., Maekawa, K., “Relationships Between Expansions and Mechanical Properties of Concrete under Coupled Freeze-Thaw Cycles and Alkali-Silica Reactions.”, The 3rd ACF Symposium, 2019.
75. Thapa, R., “Uniaxial and Biaxial Restraint in Concrete Pavement Undergoing Alkali-Silica Reaction.” Youngstown State University, Youngstown, OH, 2018.
76. Thomas M.D.A., “The Role of Calcium in Alkali-Silica Reaction.”, in Cohen M., Mindess S., Skalny J.P., “*Materials Science of Concrete*.” - The Sidney Diamond Symposium, American Ceramic Society, Westerville, OH 1998, pp. 325–331.
77. Thomas, M.D.A., “Field Studies of Fly Ash Concrete Structures Containing Reactive Aggregates.”, *Magazine of Concrete Research*, Vol. 48 (177), 1996, pp. 265-279.
78. Thomas, M.D.A., “Review of the Effect of Fly Ash and Slag on Alkali-Aggregate Reaction in Concrete.”, Building Research Establishment Report, BR314, Construction Research Communications, Watford, UK, 1996.
79. Thomas, M.D.A., Nixon, P.J., Pettifer K., “The effect of PFA on alkali–silica reaction.”, in: V.M. Malhotra (Ed.), 2nd CANMET/ACI Conference on the

Durability of Concrete, ACI SP-126 American Concrete Institute, Detroit 1991, pp. 919–940.

80. Urhan, S., "Alkali Silica and Pozzolanic Reactions in Concrete.", *Cement and Concrete Research* Vol 17 (1), 1987, pp. 141–152.
81. Villeneuve, V., Fournier, B., "Determination of the Damage in Concrete Affected by ASR - the Damage Rating index (DRI).", 14th ICAAR - International Conference on Alkali– Aggregate Reaction in Concrete, Austin, Texas, 2012.
82. Vivian, H.E., "The Effect on Mortar Expansion of Particle Size of the Reactive Component in Aggregate.", *Australian Journal of Applied Sciences* 2, 1951, pp. 488–492.
83. Walther, J.V., Helgeson, H.C., "Calculation of the Thermodynamic Properties of Aqueous Silica and the Solubility of Quartz and Its Polymorphs at High Pressures and Temperatures.", *American Journal of Science* 277 (10), 1977, pp. 1315–1351.
84. Wang, H. and Gillott, J.E., "Mechanism of Alkali-Silica Reaction and the Significance of Calcium Hydroxide." The University of Calgary, Calgary, Alberta, Canada, T2N IN4, 1991, 8pg.

7 Appendix

Table A- 1, AMBT Results for Jobe Sand.

Age (Days)	0	3	7	14	21	28
Sample Number			**Strain (%)**			
#1	0.0000	0.2735	0.3908	0.3850	0.4750	0.5395
#2	0.0000	0.2700	0.3685	0.3560	0.4430	0.5095
#3	0.0000	0.2210	0.3360	0.2925	0.3985	0.4635
#4	0.0000	0.2355	0.3485	0.3245	0.4157	0.4725
#5	0.0000	0.2485	0.3690	0.3470	0.4425	0.4945
Avg. Strain (%)	0.0000	0.2497	0.3626	**0.3410**	0.4349	0.4959

Table A- 2, AMBT Results for Non-Reactive Sand.

Age (Days)	0	3	7	14	21	28
Sample Number			**Strain (%)**			
#1	0.0000	0.0440	0.1050	0.1010	0.2015	0.2315
#2	0.0000	0.0320	0.0930	0.0885	0.1795	0.2165
#3	0.0000	0.0510	0.1120	0.1110	0.1900	0.2230
#4	0.0000	0.0275	0.0695	0.0750	0.1795	0.2230
#5	0.0000	0.0310	0.0710	0.0740	0.1525	0.2045
Avg. Strain (%)	0.0000	0.0371	0.0901	**0.0899**	0.1806	0.2197

Table A- 3, CPT Results (ASTM C1293)

Age (Days)	0	7	28	68	90	180
Sample Number			**Strain (%)**			
#1	0	0.017	0.1505	0.2685	0.3345	0.3945
#2	0	0.0255	0.114	0.2745	0.292	0.3645
#3	0	0.0135	0.1165	0.244	0.272	0.3575
#4	0	0.0145	0.124	0.246	0.3065	0.392
#5	0	0.013	0.1565	0.2665	0.2795	0.354
#6	0	0.0175	0.1175	0.2725	0.2955	0.3585
Avg. Strain (%)	**0**	**0.01683**	**0.12983**	**0.262**	**0.29667**	**0.37017**

Table A- 4, Expansion Data for B1C1 (Unrestrained Cube)

Day	X-axis avg. strain (%)	Y-axis avg. strain (%)	Z-axis avg. strain (%)	Average strain (%)
0	0.0000	0.0000	0.0000	0.0000
14	-0.0138	-0.0133	-0.0092	-0.0121
21	0.0075	0.0000	0.0025	0.0033
28	-0.0008	0.0029	0.0008	0.0010
38	-0.0050	-0.0029	0.0037	-0.0014
47	0.0004	0.0054	0.0075	0.0044
54	0.0108	0.0171	0.0133	0.0138
61	0.0233	0.0446	0.0417	0.0365
68	0.0438	0.0542	0.0483	0.0488
75	0.0542	0.0742	0.0642	0.0642
82	0.0842	0.1013	0.0958	0.0938
89	0.1179	0.1400	0.1221	0.1267
96	0.1358	0.1750	0.1579	0.1563

Table A- 5, Expansion Data for B1C2 (Unrestrained Cube)

Day	X-axis avg. strain (%)	Y-axis avg. strain (%)	Z-axis avg. strain (%)	Avg. strain (%)
0	0.0000	0.0000	0.0000	0.0000
14	-0.0087	-0.0117	-0.0004	-0.0069
21	-0.0088	-0.0087	0.0021	-0.0051
28	0.0000	-0.0042	0.0013	-0.0010
38	0.0033	-0.0087	-0.0063	-0.0039
47	0.0388	0.0113	0.0442	0.0314
54	0.0604	0.0242	0.0683	0.0510
61	0.1042	0.0696	0.1138	0.0958
68	0.1167	0.0813	0.1267	0.1082
75	0.1242	0.0913	0.1396	0.1183
82	0.1471	0.1200	0.1713	0.1461
89	0.1842	0.1563	0.2063	0.1822
96	0.2150	0.1925	0.2438	0.2171
117	0.2358	0.2204	0.2571	0.2378
135	0.2550	0.2454	0.2817	0.2607
197	0.3325	0.3538	0.3592	0.3485
218	0.3479	0.3838	0.3850	0.3722

Table A- 6, Expansion Data for B1C3 (Unrestrained Cube)

Day	X-axis avg. strain (%)	Y-axis avg. strain (%)	Z-axis avg. strain (%)	Avg. strain (%)
0	0.0000	0.0000	0.0000	0.0000
14	-0.0092	-0.0042	-0.0025	-0.0053
21	0.0075	0.0142	0.0092	0.0103
28	-0.0046	-0.0046	-0.0021	-0.0038
38	-0.0096	-0.0167	-0.0104	-0.0122
47	0.0325	0.0138	0.0271	0.0244
54	0.0454	0.0296	0.0375	0.0375
61	0.0813	0.0733	0.0742	0.0763
68	0.0979	0.0958	0.0950	0.0963
75	0.1058	0.1138	0.1025	0.1074
82	0.1204	0.1308	0.1196	0.1236
89	0.1521	0.1796	0.1579	0.1632
96	0.1746	0.2071	0.1875	0.1897
117	0.1979	0.2358	0.2171	0.2169
135	0.2196	0.2488	0.2288	0.2324
197	0.2771	0.3671	0.3213	0.3218
218	0.3100	0.4104	0.3579	0.3594
247	0.3092	0.3888	0.3908	0.3629
364	0.3917	0.4592	0.4446	0.4318
416	0.4267	0.5058	0.4925	0.4750

Table A- 7, Expansion Data of B2C1 (Uniaxially Restrained Cube)

Day	X-axis avg. strain (%)	Y-axis avg. strain (%)	Z-axis avg. strain (%)	Avg. strain (%)
0	0.0000	0.0000	0.0000	0.0000
14	-0.0267	0.0363	-0.0071	0.0008
21	-0.0146	0.0279	0.0088	0.0074
28	-0.0167	0.0042	0.0008	-0.0039
35	-0.0133	0.0029	0.0025	-0.0026
47	0.0071	0.0313	0.0229	0.0204
54	-0.0167	0.0054	0.0042	-0.0024
61	0.0200	0.0438	0.0483	0.0374
68	0.0325	0.0608	0.0538	0.0490
75	0.0121	0.0492	0.0500	0.0371
82	0.0163	0.0488	0.0525	0.0392
89	0.0171	0.0604	0.0750	0.0508
96	0.0375	0.0888	0.0846	0.0703

Table A- 8, Expansion Data of B2C2 (Uniaxially Restrained Cube)

Day	X-axis avg. strain (%)	Y-axis avg. strain (%)	Z-axis avg. strain (%)	Avg. strain (%)
0	0.0000	0.0000	0.0000	0.0000
14	0.0042	0.0050	0.0033	0.0042
21	-0.0017	0.0096	0.0033	0.0037
28	0.0000	0.0071	-0.0013	0.0019
35	-0.0050	0.0008	-0.0017	-0.0019
47	0.0108	0.0096	0.0262	0.0156
54	-0.0013	0.0154	0.0096	0.0079
61	0.0346	0.0713	0.0558	0.0539
68	0.0538	0.1133	0.0788	0.0819
75	0.0571	0.1117	0.0875	0.0854
82	0.0483	0.1288	0.0854	0.0875
89	0.0688	0.1671	0.1183	0.1181
96	0.0954	0.2163	0.1475	0.1531
117	0.1054	0.2417	0.1567	0.1679
135	0.1475	0.2971	0.1621	0.2022
197	0.1308	0.3808	0.2325	0.2481
218	0.1613	0.4279	0.2650	0.2847

Table A- 9, Expansion Data of B2C3 (Uniaxially Restrained Cube)

Day	X-axis avg. strain (%)	Y-axis avg. strain (%)	Z-axis avg. strain (%)	Avg. strain (%)
0	0.0000	0.0000	0.0000	0.0000
14	-0.0004	0.0038	0.0058	0.0031
21	-0.0063	-0.0083	0.0037	-0.0036
28	-0.0021	0.0087	0.0083	0.0050
35	-0.0046	0.0075	0.0096	0.0042
47	0.0221	0.0346	0.0321	0.0296
54	-0.0058	0.0167	0.0258	0.0122
61	0.0338	0.0475	0.0642	0.0485
68	0.0467	0.0788	0.1113	0.0789
75	0.0517	0.0996	0.1350	0.0954
82	0.0471	0.0863	0.1338	0.0890
89	0.0683	0.1292	0.1775	0.1250
96	0.0804	0.1429	0.1979	0.1404
117	0.0846	0.1625	0.2358	0.1610
135	0.1104	0.1858	0.2938	0.1967
197	0.1029	0.2125	0.3342	0.2165
218	0.1296	0.2500	0.3771	0.2522
247	0.1563	0.2758	0.4138	0.2819
364	0.1625	0.3192	0.4550	0.3122
416	0.2263	0.3654	0.5308	0.3742

Table A- 10, Expansion Date of B3C1 (Biaxially Restrained Cube)

Day	X-axis avg. strain (%)	Y-axis avg. strain (%)	Z-axis avg. strain (%)	Avg. strain (%)
0	0.0000	0.0000	0.0000	0.0000
14	0.0025	0.0054	-0.0010	0.0023
21	0.0087	0.0058	-0.0058	0.0029
28	0.0100	0.0046	-0.0088	0.0019
35	0.0067	0.0017	-0.0104	-0.0007
48	0.0558	0.0504	0.0292	0.0451
55	0.0380	0.0338	0.0077	0.0265
62	0.0750	0.0629	0.0238	0.0539
69	0.0717	0.0342	0.0121	0.0393
76	0.1104	0.0746	0.0575	0.0808
83	0.0975	0.0571	0.0183	0.0576
90	0.1283	0.0679	0.0396	0.0786
97	0.1517	0.0888	0.0521	0.0975

Table A- 11, Expansion Data of B3C2 (Biaxially Restrained Cube)

Day	X-axis avg. strain (%)	Y-axis avg. strain (%)	Z-axis avg. strain (%)	Avg. strain (%)
0	0.0000	0.0000	0.0000	0.0000
14	0.0017	0.0183	0.0133	0.0111
21	0.0021	0.0046	0.0129	0.0065
28	0.0021	0.0096	0.0163	0.0093
35	0.0058	0.0029	0.0154	0.0081
48	0.0517	0.0450	0.0550	0.0506
55	0.0346	0.0258	0.0442	0.0349
62	0.0638	0.0396	0.0550	0.0528
69	0.0633	0.0317	0.0496	0.0482
76	0.1088	0.0721	0.1000	0.0936
83	0.0838	0.0338	0.0521	0.0565
90	0.1146	0.0700	0.0871	0.0906
97	0.1271	0.0763	0.0892	0.0975
117	0.1629	0.0863	0.0913	0.1135
135	0.2504	0.1371	0.1479	0.1785
197	0.2471	0.0821	0.0858	0.1383
218	0.2913	0.0942	0.1079	0.1644

Table A- 12, Expansion Data of B3C3 (Biaxially Restrained Cube)

Day	X-axis avg. strain (%)	Y-axis avg. strain (%)	Z-axis avg. strain (%)	Avg. strain (%)
0	0.0000	0.0000	0.0000	0.0000
14	0.0042	-0.0013	0.0017	0.0015
21	0.0046	0.0042	0.0079	0.0056
28	0.0092	0.0029	0.0100	0.0074
35	0.0017	0.0008	0.0067	0.0031
48	0.0592	0.0475	0.0150	0.0406
55	0.0413	0.0283	-0.0233	0.0154
62	0.0625	0.0467	-0.0054	0.0346
69	0.0667	0.0400	-0.0150	0.0306
76	0.0963	0.0663	-0.0104	0.0507
83	0.0800	0.0358	-0.0046	0.0371
90	0.1388	0.0517	-0.0173	0.0577
97	0.1458	0.0750	0.0213	0.0807
117	0.1779	0.0754	0.0292	0.0942
135	0.2225	0.1033	0.0388	0.1215
197	0.2563	0.0675	-0.0167	0.1024
218	0.2900	0.0917	0.0062	0.1293
247	0.3425	0.1042	0.0058	0.1508
364	0.4029	0.1392	0.0333	0.1918
416	0.4558	0.1367	0.0583	0.2169

Table A- 13, Axially Avg. Strain for Unrestrained Cubes

Day	X-axis avg. strain (%)	Y-axis avg. strain (%)	Z-axis avg. strain (%)
0	0.0000	0.0000	0.0000
14	-0.0106	-0.0097	-0.0040
21	0.0021	0.0018	0.0046
28	-0.0018	-0.0019	0.0000
35	-0.0038	-0.0094	-0.0043
48	0.0239	0.0101	0.0263
55	0.0389	0.0236	0.0397
62	0.0696	0.0625	0.0765
69	0.0861	0.0771	0.0900
76	0.0947	0.0931	0.1021
83	0.1172	0.1174	0.1289
90	0.1514	0.1586	0.1621
97	0.1751	0.1915	0.1964
117	0.2169	0.2281	0.2371
135	0.2373	0.2471	0.2552
197	0.3048	0.3604	0.3402
218	0.3290	0.3971	0.3715
247	0.3092	0.3888	0.3908
364	0.3917	0.4592	0.4446
416	0.4267	0.5058	0.4925

Table A- 14, Axially Avg. Strain for Uniaxially Restrained Cubes

Day	X-axis avg. strain (%)	Y-axis avg. strain (%)	Z-axis avg. strain (%)
0	0.0000	0.0000	0.0000
14	-0.0076	0.0150	0.0007
21	-0.0075	0.0097	0.0053
28	-0.0063	0.0067	0.0026
35	-0.0076	0.0037	0.0035
48	0.0133	0.0251	0.0271
55	-0.0079	0.0125	0.0132
62	0.0294	0.0542	0.0561
69	0.0443	0.0843	0.0813
76	0.0403	0.0868	0.0908
83	0.0372	0.0879	0.0906
90	0.0514	0.1189	0.1236
97	0.0711	0.1493	0.1433
117	0.0950	0.2021	0.1963
135	0.1290	0.2415	0.2279
197	0.1169	0.2967	0.2833
218	0.1454	0.3390	0.3210
247	0.1563	0.2758	0.4138
364	0.1625	0.3192	0.4550
416	0.2263	0.3654	0.5308

Table A- 15, Axially Avg. Strain for Biaxially Restrained Cubes.

Day	X-axis avg. strain (%)	Y-axis avg. strain (%)	Z-axis avg. strain (%)
0	0.0000	0.0000	0.0000
14	0.0047	0.0075	0.0028
21	0.0050	0.0049	0.0051
28	0.0058	0.0057	0.0071
35	0.0039	0.0018	0.0047
48	0.0331	0.0476	0.0556
55	0.0095	0.0293	0.0379
62	0.0244	0.0497	0.0671
69	0.0156	0.0353	0.0672
76	0.0490	0.0710	0.1051
83	0.0219	0.0422	0.0871
90	0.0364	0.0632	0.1272
97	0.0542	0.0800	0.1415
117	0.0602	0.0808	0.1704
135	0.0933	0.1202	0.2365
197	0.0346	0.0748	0.2517
218	0.0571	0.0929	0.2906
247	0.0058	0.1042	0.3425
364	0.0333	0.1392	0.4029
416	0.0583	0.1367	0.4558

Table A- 16, Volumetric Strain for All Stress States.

Day	Volumetric Strain for Unrestrained Cubes (%)	Volumetric Strain for Uniaxially Restraint Cubes (%)	Volumetric Strain for Biaxially Restraint Cubes (%)
0	0.0000	0.0000	0.0000
14	-0.0243	0.0081	0.0149
21	0.0085	0.0075	0.0150
28	-0.0038	0.0031	0.0186
35	-0.0175	-0.0004	0.0104
48	0.0603	0.0656	0.1363
55	0.1022	0.0178	0.0768
62	0.2086	0.1397	0.1413
69	0.2532	0.2099	0.1181
76	0.2899	0.2179	0.2251
83	0.3635	0.2157	0.1513
90	0.4721	0.2939	0.2269
97	0.5631	0.3638	0.2757
117	0.6821	0.4933	0.3115
135	0.7396	0.5983	0.4500
197	1.0054	0.6969	0.3610
218	1.0975	0.8054	0.4406
247	1.0888	0.8458	0.4525
364	1.2954	0.9367	0.5754
416	1.4250	1.1225	0.6508

Table A- 17, Number of Cracks Found in Unrestrained Cubes.

Plane	Age (Days)	Crack Type						
		CCA	OCA	OCAG	CAD	DAP	CCP	CCPG
B1C1 X(0)	97	178	72	0	214	12	142	4
B1C1 Y(0)		177	79	2	235	16	212	11
B1C1 Z(0)		184	86	1	235	17	188	5
B1C2 X(0)	152	275	11	5	13	81	194	12
B1C2 Y(0)		275	10	1	5	86	253	1
B1C2 Z(0)		272	17	0	15	64	346	0
B1C3 X(0)	416	195	11	0	12	65	292	0
B1C3 Y(0)		164	5	0	6	32	259	0
B1C3 Z(0)		201	14	0	8	67	282	0

Table A- 18, Number of Cracks in Uniaxially Restrained Cubes.

Plane	Age (Days)	Crack Type						
		CCA	OCA	OCAG	CAD	DAP	CCP	CCPG
B2C1 X(5 MPa)	97	217	47	0	110	16	26	1
B2C1 Y(0)		217	31	0	116	15	16	1
B2C1 Z(0)		189	34	0	103	8	25	0
B2C3 X(5 MPa)	152	171	4	0	3	20	146	0
B2C2 Y(0)		206	11	0	1	52	106	0
B2C2 Z(0)		176	8	0	0	34	156	0
B2C3 X(5 MPa)	416	179	18	0	10	34	414	0
B2C3 Y(0)		165	10	0	3	20	319	0
B2C3 Z(0)		152	10	0	1	66	131	0

Table A- 19, Number of Cracks in Biaxially Restrained Cubes.

Plane	Age (Days)	Crack Type						
		CCA	OCA	OCAG	CAD	DAP	CCP	CCPG
B3C1 X(5 MPa)	97	245	57	0	83	15	19	0
B3C1 Y(4 MPa)		225	45	0	106	18	20	0
B3C1 Z(0)		234	52	1	89	17	29	0
B3C2 X(5 MPa)	152	161	9	0	4	22	127	0
B3C2 Y(4 MPa)		156	5	0	0	28	91	0
B3C2 Z(0)		195	2	0	6	26	60	0
B3C3 X(5 MPa)	416	164	2	0	8	9	203	0
B3C3 Y(4 MPa)		142	5	0	0	29	135	0
B3C3 Z(0)		155	5	0	3	39	69	0